Title	State-space modelling for the ejector-based refrigeration system driven by low grade energy
Author(s)	Xue, Binqiang; Cai, Wenjian; Wang, Xinli
Citation	Xue, B., Cai, W., & Wang, X. (2015). State-space modelling for the ejector-based refrigeration system driven by low grade energy. Applied thermal engineering, 75, 430-444.
Date	2014
URL	http://hdl.handle.net/10220/25456
Rights	© 2014 Elsevier Ltd. This is the author created version of a work that has been peer reviewed and accepted for publication by Applied Thermal Engineering, Elsevier Ltd. It incorporates referee's comments but changes resulting from the publishing process, such as copyediting, structural formatting, may not be reflected in this document. The published version is available at: [http://dx.doi.org/10.1016/j.applthermaleng.2014.09.037].

State-space modelling for the ejector-based refrigeration system driven by low grade energy

Binqiang Xue[a,b], Wenjian Cai [a,*], Xinli Wang[a,c]

[a]*EXQUISITUS, Centre for E-City, School of Electrical and Electronic Engineering, Nanyang Technological University, Singapore 639798*

[b]*Department of Control Engineering, College of Automation Engineering, Qingdao University, Qingdao 266071, China*

[c]*State Key Laboratory of Industrial Control Technology, Department of Control Science and Engineering, Zhejiang University, Hangzhou 310027, China*

Abstract: This paper presents a novel global state-space model to describe the ejector-based refrigeration system, which includes the dynamics of the two heat exchangers and the static properties of ejector, compressor and expansion valve. Different from the existing methods, the proposed method introduces some intermediate variables into the dynamic modelling in developing reduced order models of the heat exchangers (evaporator and condenser) based on the Number of Transfer Units (NTU) method. This global model with fewer dimensions is much simpler and can be more convenient for the real-time control system design, compared with other dynamic models. Finally, the proposed state-space model has been validated by dynamic response experiments on the ejector-based refrigeration cycle with refrigerant R134a.The experimental results indicate that the proposed model can predict well the dynamics of the ejector-based refrigeration system.

Keywords: Ejector-based refrigeration system, Modelling, Number of Transfer Units method (NTU), Experiment

1. Introduction

With the rapid development of the society, the shortage of energy and pollution of the environment become increasingly serious. Faced with this situation, the potential of exploiting waste heat and low grade energy from industrial process, automobiles, geothermal and solar energies can be a promising alternative in view of ever increasing energy demand and environmental burdens. For these reasons, recent years have witnessed an increasing interest in the study of low grade thermal energy for refrigeration and air conditioning systems.

Among these systems, ejector-based refrigeration systems [1-5] driven by low-grade waste heat have attracted great attentions from research community, since the ejector has some properties of no moving parts, no electricity power consumption and relatively low cost. However, compared with the conventional refrigeration system, the introduction of the ejector highly complicates the thermo-fluid dynamics of refrigerant in the ejector-based refrigeration system and leads to difficulty in regulating its operating conditions to meet the space cooling requirements. Therefore, it is of necessity to adequately understand the dynamic response by developing a global dynamic model of the system including both the ejector and conventional refrigeration cycle.

* Corresponding author. Tel: +65 6790 6862; fax: +65 6793 3318; email: ewjcai@ntu.edu.sg

Currently, a great number of studies focused on the ejector performance prediction and ejector modelling [1-5]. Zhu et al. [1] developed a simplified hybrid model to determine the ejector performance, but they did not consider the pressure at outlet of the ejector and give the relationship between the outlet pressure and the primary/secondary flow pressure. He et al. [2] indicated that these models of the ejectors can be classified as thermodynamic model, dynamic model, empirical/semi-empirical model, each of which has respective characters. Lin et al. [3] used the Computational Fluid Dynamics (CFD) technique to develop the ejector model and investigate the influences of cooling load on the Pressure Recovery Ratio (PRR) performance. Different from the method [3], Chou et al. [4] developed empirical model for predicting the maximum flow ratio of the ejector, by using the multi-parameter equation. Compared with the above ejector models, Chen et al. [5] developed a new 1D model for performance prediction of the ejector at critical and subcritical operating condition, and analysed the pressure at the exit of the diffuser. This kind of the 1D model with cheap computation will be adopted in present study, because of easy integration into the model of the conventional refrigeration cycle.

In addition, the dynamic modelling of the conventional refrigeration cycle on the balance between complexity and model accuracy is also a hot research topic [6-15]. Two methods for modelling heat exchangers are adopted in system modelling, including finite-volume [6-7] and moving-boundary lumped-parameter methods [8-15]. Using finite-volume method, Jahangeer et al. [6] decomposed heat exchanger geometry into finite regions where spatial effects are captured, but complexity is introduced due to spatially varying flow and heat transfer. Bendapudi et al. [7] developed a validated system model for a centrifugal chiller to capture its transient performance using finite-volume method. In contrast to these finite-volume models, lumped-parameter models have many merits such as reducing complexity, less computation and good theoretic background by considering position of refrigerant phase change and considering lumped heat transfer parameters of each fluid phase region. Hence, many scholars employed this method to study simple models of heat exchangers for control system design. He at al. [9] presented a novel lumped-parameter model to represent dynamics of the vapour compression cycle, based on a moving-interface approach. Following this work, Rasmussen [10] put forward a highly nonlinear state space model based on first principles and experimental results validated its effectiveness. Following the basic ideas of [7], Bendapudi et al. [11] further discussed development and analysis of two methods applied to a flooded evaporator and condenser. Furthermore, a comprehensive understand about the trade-off between finite-volume and moving-boundary methods were given. Li et al. [12] extended their works and introduced some switching schemes between different formulations and pseudo-state variables to derive the transitions of dynamical states from heat exchangers during stop-start transients. Based on this idea, Catano [13] developed a

lumped-parameter modelling method for electronics cooling by imposing heat flux boundary condition to evaporator. Furthermore, this proposed model was compared with experimental results at multiple operating conditions. Recently, Yao et al. [14] transformed the ODEs describing dynamics of a chiller into state-space form, by using vector-matrix notation and linearization. Later on, Ding et al. [15] also proposed a hybrid modelling approach for dynamics of condenser, by packing some system variables into less unknown parameters obtained by experimental data using least squares methods.

Although the models of the ejectors and the conventional refrigeration cycles were studied, global dynamic models of the ejector-based refrigeration systems are hardly considered. That is, all the component models are not integrated into a uniform mathematic representation. Furthermore, the above dynamic modelling of the conventional refrigeration cycles considered refrigerant mass flow rates at boundary interfaces, rather than taking into account the variations of the refrigerant mass flow rates in multiple fluid phase regions. This may reduce modelling accuracy due to the loss of some important information on reflecting the dynamics of refrigerant mass flow rates in multiple fluid phase regions.

In this paper, we present a global low-order state-space model of the ejector-based refrigeration system. Much different from the above dynamic models of heat exchangers, reduced-order nonlinear models of evaporator and condenser are respectively developed based on the NTU method by introducing some intermediate variables to describe the variations of refrigerant mass flow rates in multiple fluid phase regions. These two dynamic models are capable of revealing essentially the dynamic characteristics of each of the fluid phase regions and providing much more information to describe the phase changes of the refrigerant, since more physical parameters are fully taken into account. Combing a1D static model of the ejector with two dynamic models of heat exchangers, a global nonlinear state-space model of the ejector-based refrigeration system is obtained. Finally, experimental validation with R134a is carried out based on the real-time experimental test rig. The results show that the proposed model has a good performance in predicting the dynamics of the system and is beneficial for the real-time control and optimization of the ejector-based refrigeration system.

2. System description

The refrigeration system studied in this paper is a basic vapor compression cycle integrated with an ejector cycle driven by low grade energy. The schematic figures shown in Fig. 1 and Fig. 2 illustrate the change of the refrigerant states during the cycle in pressure-enthalpy chart. Refrigerant vapour with high pressure and high temperature at state ‘1’ is cooled in the condenser by rejecting heat to surrounding air. The condensed refrigerant at state ‘2’ is divided into two parts: one part brought into the generator by a

liquid pump and the other part entering the expansion valve. On one hand, the liquid refrigerant at state ‘3’ is heated into vapor state by utilizing the heat sources such as solar energy, low grade waste heat from automobile and industries. Then the superheated refrigerant at state ‘4’ with high pressure and temperature enters the converging – diverging nozzle of the ejector acting as the primary flow. On the other hand, the two-phase refrigerant at state ‘5’ from the expansion valve provides a cooling effect in the evaporator by absorbing heat from the occupants’ space. As the refrigerant in gas phase enters compressor at state ‘6’, it is compressed to be higher-pressure state, accompanying with higher temperature. Since supersonic vapour generated at the nozzle outlet gives rise to a low pressure region in the suction chamber, the refrigerant at state ‘7’called the secondary flow from compressor can be entrained into the ejector. Then, the primary flow and the entrained flow mix and can be compressed to be a whole flow with high condensing pressure in the diffuser. Finally, mixed stream at state ‘1’ leaving the ejector returns to the condenser.

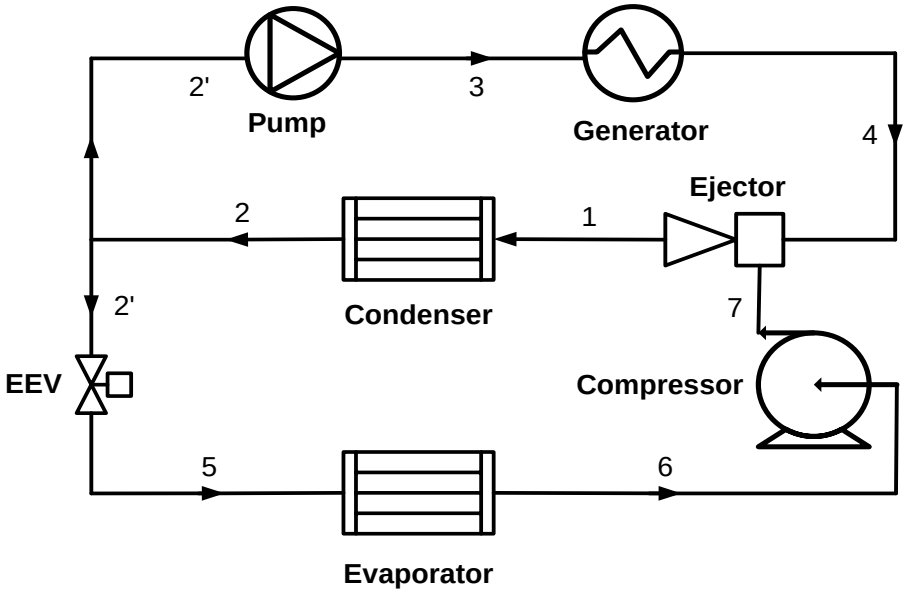

Fig. 1. A simplified schematic of an ejector-based refrigeration system

Among the refrigerants with relatively high condensing pressure for ejector-based refrigeration systems such as R134a, R245fa and R365mfc, several advantages of R134a are as follows: (a) Zero Ozone Depletion Potential (ODP); and (b) much higher condensing pressure (8.87 bar) than those of R245fa (2.13 bar) and R365mfc (0.69 bar) around a condensing temperature 35 ℃. However, it is difficult to select a proper liquid pump with high boost pressure to generate the high generator pressure. Therefore, environmentally friendly refrigerant 134a with the high condensing pressure is used for the designed ejector-based refrigeration system.

In addition, due to the limitation of the operating condition, evaporating pressure ranging from 2.5 bar to 4.3 bar is much lower than condensing pressure around 9.0 bar in this paper. Only depending on the ejector

can't compress the refrigerant with the low evaporating pressure to the one with the higher condensing pressure, so a variable-speed compressor is introduced, different from the design structures of other ejector-based cooling systems. It is noted that the ejector can be used for recovering the waste heat energy and reduces the electric power consumption of the compressor, which can be beneficial for improving system performance of the ejector-based refrigeration system, compared with the conventional compression refrigeration system [10].

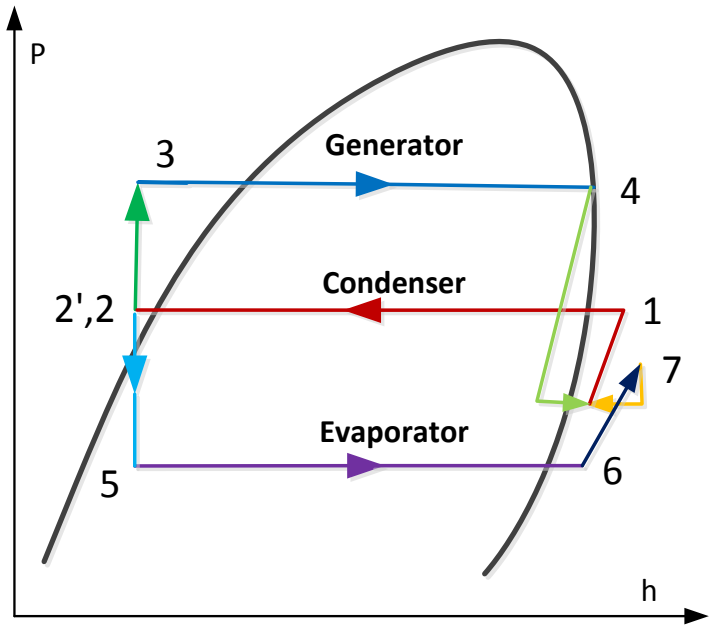

Fig. 2. P-h diagram of the ejector refrigeration system

3. System modelling

The ejector-based refrigeration system in study mainly consists of five components, namely evaporator, condenser, ejector, compressor and expansion valve. These component models can be separated into dynamic or static ones relying on their response speeds. Ejector, compressor and expansion valve are usually modelled using static equations involving some empirical formulas [9]. Dynamic modelling of the heat exchangers has been always a hot topic, due to the disadvantages of the existing models such as complexity and high order which are not suitable for system level designs and real-time control demands. Therefore, more emphasis will be put on building low-order dynamic models of the heat exchangers in this work, which not only captures the dominant dynamic behaviour of the refrigeration cycle, but also makes a trade-off between dynamic complexity and modelling accuracy.

3.1. Dynamic model of the heat exchangers

Dynamic behaviors of the ejector based refrigeration cycle can be dominated by evaporator and condenser. These heat exchangers can be modelled based on the laws of mass and energy conservation, by using a lumped-parameter and moving-boundary method accounting for different fluid phase regions. Although some steady-state models of the heat exchangers were presented by researchers, they can be considered as special cases of the dynamical modeling under special operating conditions [16].

3.1.1. Evaporator

According to the states of the refrigerant in the evaporator, the evaporator can be divided into two regions: a two-phase region and a superheated vapour region. Then, a simpler dynamic model of the evaporator will be presented based on the conservation of the mass and energy by introducing two intermediate variables to capture the dynamic characteristics of the two fluid phase regions instead of the original boundary interface variable $\dot{m}_{\text{int}}$ [10], and using the NTU method [8] detailed in the following condenser section to calculate the heat transfer rates between the refrigerant and the tube wall in the two phase regions.

A. Conservation of mass and energy in two-phase region

By considering average refrigerant mass flow rate and heat transfer rate in two-phase region, governing partial differential equations for refrigerant mass and energy conversation could be simplified into

$$\frac{\partial(\rho_{e1}A_e)}{\partial t}+\frac{\partial \dot{m}}{\partial z}=0 \tag{1}$$

$$\frac{\partial(\rho_{e1}A_e h_{e1}-A_e P_e)}{\partial t}+\frac{\partial\left(\dot{m}h_{e1}\right)}{\partial z}=\frac{\partial Q_{etp}}{\partial z} \tag{2}$$

where $\dot{m}$, ρ_{e1} and h_{e1} are the refrigerant mass flow rate, density and enthalpy in the two-phase region, respectively; P_e is the evaporating pressure; A_e is the cross-sectional area of the evaporator; Q_{etp} is the heat transfer rate between the refrigerant and the tube wall in two-phase region.

When the flow is two-phase, void fraction $\gamma=\frac{V_g}{V}$ is defined as the ratio of vapour volume V_g to total volume V [10], and some void fraction models have been used to describe certain characteristics of a two-phase flow. A detailed model of the void fraction can be found in [17]. The mean void fraction is defined as $\gamma_e=\frac{1}{L_{e1}}\int_0^{L_{e1}}\gamma dz$. Many references studied the dynamic modelling of the heat exchangers based on the assumption that the value of the mean void fraction is invariant with time for small transients. However, it

cannot be fit for conditions when the fluid at the exit of heat exchanger is two-phase. In this paper, a constant mean void fraction is used for simplifying the modelling process of heat exchangers within an acceptable approximation. Furthermore, due to the mean void fraction used in the calculation of the vapour volume, the mean mass flow rate of two-phase refrigerant can be easily derived in the form of the saturated liquid and vapour densities and total volume. Then, the density in two-phase region can be expressed as $\rho_{e1} = \gamma_e \rho_{eg} + (1-\gamma_e)\rho_{ef}$. Applying Leibniz's rules

$$\int_{x_1(t)}^{x_2(t)} \frac{\partial f(x,t)}{\partial t} dz = \frac{d}{dt} \int_{x_1(t)}^{x_2(t)} f(x,t)dz + f(x_1(t),t)\frac{dx_1(t)}{dt} - f(x_2(t),t)\frac{dx_2(t)}{dt}$$

and integrating each term of equation (1) over the length L_{e1} of the two-phase region, it easily obtains

$$\int_0^{L_{e1}} \left(\frac{\partial(\rho_{e1}A_e)}{\partial t} + \frac{\partial \dot{m}_{e1}}{\partial z} \right) dz = \left(\frac{d\rho_{ef}}{dP_e}(1-\gamma_e) + \frac{d\rho_{eg}}{dP_e}\gamma_e \right) A_e L_{e1} \dot{P}_e + (\rho_{ef} - \rho_{eg})(1-\gamma_e) A_e \dot{L}_{e1} + \Delta \dot{m}_{e1} = 0 \quad (3)$$

where $\Delta \dot{m}_{e1} = \dot{m}_{z=L_{e1}} - \dot{m}_{z=0}$, ρ_{ef} and ρ_{eg} are the variation of the refrigerant mass flow rate in the two-phase region, the saturated liquid and vapour densities of the refrigerant at evaporating pressure P_e, respectively. Furthermore, $\Delta \dot{m}_{e1}$ describes the dynamics of the refrigerant mass flow rate in two-phase region, instead of the mass flow rate at the boundary interface of the evaporator.

Furthermore, based on the energy conservation, each term of this equation (2) is integrated over the length L_{e1} of the two-phase region. Integrating the first term and applying Leibniz's rules results in

$$\begin{aligned} &\int_0^{L_{e1}} \frac{\partial(\rho_{e1}A_e h_{e1} - A_e P_e)}{\partial t} dz \\ &= \left(\frac{d(\rho_{ef}h_{ef})}{dP_e}(1-\gamma_e) + \frac{d(\rho_{eg}h_{eg})}{dP_e}\gamma_e \right) A_e L_{e1} \dot{P}_e + (\rho_{ef}h_{ef} - \rho_{eg}h_{eg})(1-\gamma_e) A_e \dot{L}_{e1} - A_e L_{e1} \dot{P}_e \end{aligned} \quad (4)$$

where h_{ef} and h_{eg} are the saturated liquid and vapour enthalpies of the refrigerant at evaporating pressure P_e, respectively. Integrating the rest of the equation (2) results in

$$\int_0^{L_{e1}} \left(\frac{\partial\left(\dot{m}h_{e1} - Q_{etp}\right)}{\partial z} \right) dz = (\dot{m}_{ei} + \Delta \dot{m}_{e1})h_{eg} - \dot{m}_{ei}h_{ei} - Q_{etp} \quad (5)$$

where $\dot{m}_{ei}$ is the refrigerant mass flow rate at the evaporator inlet; Q_{etp} can be evaluated by the NTU method [9] more detailed in the next section. Combing the equations (4) and (5) results in

$$\left(\frac{d(\rho_{ef}h_{ef})}{dP_e}(1-\gamma_e) + \frac{d(\rho_{eg}h_{eg})}{dP_e}\gamma_e - 1 \right) A_e L_{e1} \dot{P}_e + (\rho_{ef}h_{ef} - \rho_{eg}h_{eg})(1-\gamma_e) A_e \dot{L}_{e1} + \dot{m}_{ei}(h_{eg} - h_{ei}) + \Delta \dot{m}_{e1}h_{eg} = Q_{etp} \quad (6)$$

B. Conservation of mass and energy in superheat region

Similar to the above descriptions in two-phase region, the integrations of partial differential equations for the conservation of the refrigerant mass and energy are given by

$$\int_{L_{e1}}^{L_{eT}} \left(\frac{\partial(\rho_{e2} A_e)}{\partial t} + \frac{\partial \dot{m}}{\partial z} \right) dz = \left(\frac{\partial \rho_{e2}}{\partial P_e} + \frac{1}{2} \frac{\partial \rho_{e2}}{\partial h_{e2}} \frac{dh_{eg}}{dP_e} \right) A_e L_{e2} \dot{P}_e + \frac{1}{2} \frac{\partial \rho_{e2}}{\partial h_{e2}} A_e L_{e2} \dot{h}_{eo} + (\rho_{eg} - \rho_{e2}) A_e \dot{L}_{e1} + \Delta \dot{m}_{e2} = 0 \tag{7}$$

$$\begin{aligned} &\left(\frac{1}{2} \frac{dh_{eg}}{dP_e} \rho_{e2} + (\frac{\partial \rho_{e2}}{\partial P_e} + \frac{1}{2} \frac{\partial \rho_{e2}}{\partial h_{e2}} \frac{dh_{eg}}{dP_e}) h_{e2} - 1 \right) A_e L_{e2} \dot{P}_e + \frac{1}{2} \left(\frac{\partial \rho_{e2}}{\partial h_{e2}} h_{e2} + \rho_{e2} \right) A_e L_{e2} \dot{h}_{eo} \\ &\qquad + (\rho_{eg} h_{eg} - \rho_{e2} h_{e2}) A_e \dot{L}_{e1} + \dot{m}_{eo} (h_{eo} - h_{eg}) + \Delta \dot{m}_{e2} h_{eg} = Q_{esp} \end{aligned} \tag{8}$$

where $\Delta \dot{m}_{e2} = \dot{m}_{z=L_{eT}} - \dot{m}_{z=L_{e1}}$, ρ_{e2} and h_{e2} are the variation of the refrigerant mass flow rate, density and enthalpy in superheat region, respectively; h_{eg} and h_{eo} are the saturated vapour and outlet enthalpies, respectively; $\dot{m}_{eo}$ is the refrigerant mass flow rate at the evaporator outlet; Q_{esp} is the heat transfer rate between the refrigerant and the tube wall in superheat region (see Appendix A for the calculations of partial differential equations in superheat region of the evaporator).

C. Governing ordinary differential equations

Different from other dynamic models described by [8-15], a unique characteristic of the proposed modelling method in this work lies in the following description

$$\int_0^{L_{eT}} \frac{\partial \dot{m}}{\partial z} dz = \int_0^{L_{e1}} \frac{\partial \dot{m}}{\partial z} dz + \int_{L_{e1}}^{L_{eT}} \frac{\partial \dot{m}}{\partial z} dz \tag{9}$$

Integrating each term of equation (9), it easily obtains

$$\dot{m}_{eo} - \dot{m}_{ei} = \Delta \dot{m}_{e1} + \Delta \dot{m}_{e2} \tag{10}$$

This equation (10) indicates that the sum of the dynamics of the refrigerant mass flow rates in two regions can equal to the difference between refrigerant mass flow rates at the inlet and outlet of the evaporator. $\Delta \dot{m}_{e1}$ and $\Delta \dot{m}_{e2}$ are used to describe the variations of the refrigerant mass flow rate in two fluid phase regions, rather than utilizing the refrigerant mass flow rate difference between the boundary interfaces of fluid phase regions and inlet/outlet of the evaporator [10].

Combing equations (3), (7) and (10) yields

$$\left(\frac{d\rho_{ef}}{dP_e}L_{e1}(1-\gamma_e)+\frac{d\rho_{eg}}{dP_e}L_{e1}\gamma_e+\frac{\partial\rho_{e2}}{\partial P_e}L_{e2}+\frac{1}{2}\frac{\partial\rho_{e2}}{\partial h_{e2}}\frac{\partial h_{eg}}{\partial P_e}L_{e2}\right)A_e\dot{P}_e$$
$$+\frac{1}{2}\frac{\partial\rho_{e2}}{\partial h_{e2}}A_eL_{e2}\dot{h}_{eo}+\left((\rho_{ef}-\rho_{eg})(1-\gamma_e)+(\rho_{eg}-\rho_{e2})\right)A_e\dot{L}_{e1}=\dot{m}_{ei}-\dot{m}_{eo} \quad (11)$$

Deriving two variables $\Delta\dot{m}_{e1}$ and $\Delta\dot{m}_{e2}$ from equations (3) and (7), and substituting them into equations (6) and (8) respectively, those equations can become

$$\left(\frac{d(\rho_{ef}h_{ef})}{dP_e}(1-\gamma_e)+\frac{d(\rho_{eg}h_{eg})}{dP_e}\gamma_e-1\right)A_eL_{e1}\dot{P}_e+(\rho_{ef}h_{ef}-\rho_{eg}h_{eg})(1-\gamma_e)A_e\dot{L}_{e1}=\dot{m}_{ei}(h_{ei}-h_{eg})+Q_{etp} \quad (12)$$

$$\left((\frac{\partial\rho_{e2}}{\partial P_e}+\frac{1}{2}\frac{\partial\rho_{e2}}{\partial h_{e2}}\frac{dh_{eg}}{dP_e})(h_{e2}-h_{eg})+\frac{1}{2}\frac{dh_{eg}}{dP_e}\rho_{e2}-1\right)A_eL_{e2}\dot{P}_e+\frac{1}{2}\left(\frac{\partial\rho_{e2}}{\partial h_{e2}}(h_{e2}-h_{eg})+\rho_{e2}\right)A_eL_{e2}\dot{h}_{eo}$$
$$+\rho_{e2}(h_{eg}-h_{e2})A_e\dot{L}_{e1}=\dot{m}_{eo}(h_{eg}-h_{eo})+Q_{esp} \quad (13)$$

In other words, replacing the boundary interface variable $\dot{m}_{e\text{int}}$ proposed by [10], the two intermediate variables $\Delta\dot{m}_{e1}$ and $\Delta\dot{m}_{e2}$ can give more comprehensive understanding of the refrigerant mass flow rate in fluid regions, although the similar results are obtained. Combing the equations (11) - (13), the governing equations for evaporator dynamics can be expressed by a nonlinear state space form shown below:

$$\dot{x}_e=Z_e^{-1}(x_e)f(x_e,u_e) \quad (14)$$

with system state $x_e=\begin{bmatrix}L_{e1} & P_e & h_{eo}\end{bmatrix}^T$, system input $u_e=\begin{bmatrix}\dot{m}_{ei} & \dot{m}_{eo}\end{bmatrix}^T$ and system noise $w_e=[Q_{etp} \quad Q_{esp}]$, where $f(x_e,u_e)$ and $Z_e(x_e)$ are obtained from

$$f(x_e,u_e)=\begin{bmatrix}\dot{m}_{ei}(h_{ei}-h_{eg})+Q_{etp}\\ \dot{m}_{eo}(h_{eg}-h_{eo})+Q_{esp}\\ \dot{m}_{ei}-\dot{m}_{eo}\end{bmatrix},\quad Z_e(x_e)=\begin{bmatrix}e_{11} & e_{12} & 0\\ e_{21} & e_{22} & e_{23}\\ e_{31} & e_{32} & e_{33}\end{bmatrix}$$

and the elements of matrix $Z_e(x_e)$ are shown in Table 1.

Table 1 Elements of matrix $Z_e(x_e)$

e_{11}	$\rho_{ef}(h_{ef}-h_{eg})(1-\gamma_e)A_e$
e_{12}	$\left((\frac{d(\rho_{ef}h_{ef})}{dP_e}-\frac{d\rho_{ef}}{dP_e}h_{eg})(1-\gamma_e)+(\frac{d(\rho_{eg}h_{eg})}{dP_e}-\frac{d\rho_{eg}}{dP_e}h_{eg})\gamma_e-1\right)A_eL_{e1}$
e_{21}	$\rho_{e2}\left(h_{eg}-h_{e2}\right)A_e$
e_{22}	$\left((\frac{\partial\rho_{e2}}{\partial P_e}+\frac{1}{2}\frac{\partial\rho_{e2}}{\partial h_{e2}}\frac{dh_{eg}}{dP_e})(h_{e2}-h_{eg})+\frac{1}{2}\frac{dh_{eg}}{dP_e}\rho_{e2}-1\right)A_eL_{e2}$

e_{23}	$\frac{1}{2}\left(\frac{\partial \rho_{e2}}{\partial h_{e2}}(h_{e2}-h_{eg})+\rho_{e2}\right)A_e L_{e2}$
e_{31}	$\left((\rho_{eg}-\rho_{e2})+(\rho_{ef}-\rho_{eg})(1-\gamma_e)\right)A_e$
e_{32}	$\left((\frac{\partial \rho_{e2}}{\partial P_e}+\frac{1}{2}\frac{\partial \rho_{e2}}{\partial h_{e2}}\frac{dh_{eg}}{dP_e})L_{e2}+\frac{d\rho_{ef}}{dP_e}L_{e1}(1-\gamma_e)+\frac{d\rho_{eg}}{dP_e}\gamma_e L_{e1}\right)A_e$
e_{33}	$\frac{1}{2}\frac{\partial \rho_{e2}}{\partial h_{e2}}A_e L_{e2}$

Compared with the dynamic models proposed by [10] where the tube wall temperatures as the state variables were considered in the state space models of the heat exchangers, a new much simpler model of the evaporator has been presented by employing the NTU method to evaluate the heat transfer rate between the refrigerant and the tube wall instead of calculating the tube wall temperatures at the cost of the model accuracy. More details about the algorithm of the NTU method will be described in the following section. Furthermore, the proposed model has introduced two intermediate variables $\Delta\dot{m}_{e1}$ and $\Delta\dot{m}_{e2}$ to describe the dynamics of the refrigerant mass flow rates in multiple fluid phase regions instead of the original boundary-interface variable [10], which provides much more information to describe the phase changes of the refrigerant, since more physical parameters are fully taken into account.

3.1.2. Condenser

Similar to the evaporator model, the condenser also is divided into three parts including a superheat region, a two-phase region and a subcool region. First of all, three dynamic variables $\Delta\dot{m}_{c1}, \Delta\dot{m}_{c2}$ and $\Delta\dot{m}_{c3}$ are introduced to represent the refrigerant mass flow rates in the three regions, respectively. Next, the NTU method is used to evaluate the heat transfer rate between the refrigerant and the tube wall. Finally, a simpler model of the condenser can be derived based on the conservation of the mass and energy as follows.

A. Conservation of mass and energy in superheat region

By introducing the variation of the refrigerant mass flow rate $\Delta\dot{m}_{c1}$ in superheat region, the mass and energy conservation equations in superheat region can be calculated respectively as

$$\left(\frac{\partial \rho_{c1}}{\partial P_c}+\frac{1}{2}\frac{\partial \rho_{c1}}{\partial h_{c1}}\frac{dh_{cg}}{dP_c}\right)A_c L_{c1}\dot{P}_c+\frac{1}{2}\frac{\partial \rho_{c1}}{\partial h_{c1}}A_c L_{c1}\dot{h}_{ci}+(\rho_{c1}-\rho_{cg})A_c\dot{L}_{c1}+\Delta\dot{m}_{c1}=0 \tag{15}$$

$$\begin{aligned}\left((\frac{\partial \rho_{c1}}{\partial P_c}+\frac{1}{2}\frac{\partial \rho_{c1}}{\partial h_{c1}}\frac{dh_{cg}}{dP_c})h_{c1}+\frac{1}{2}\frac{dh_{cg}}{dP_c}\rho_{c1}-1\right)A_c L_{c1}\dot{P}_c+\frac{1}{2}\left(\frac{\partial \rho_{c1}}{\partial h_{c1}}h_{c1}+\rho_{c1}\right)A_c L_{c1}\dot{h}_{ci}\\ +(\rho_{c1}h_{c1}-\rho_{cg}h_{cg})A_c\dot{L}_{c1}+\dot{m}_{ci}(h_{cg}-h_{ci})+\Delta\dot{m}_{c1}h_{cg}=Q_{csp}\end{aligned} \tag{16}$$

where h_{ci} and h_{co} are refrigerant inlet and outlet enthalpies of condenser, respectively; h_{c1} and ρ_{c1} are the refrigerant enthalpy and density in superheat region, respectively; h_{cf} and h_{cg} are the saturated liquid and vapour enthalpies of the refrigerant at condensing pressure P_c, respectively; $\dot{m}_{ci}$ is the refrigerant mass flow rate at the condenser inlet and $\Delta\dot{m}_{c1} = \dot{m}_{z=L_{c1}} - \dot{m}_{z=0}$ is the variation of the refrigerant mass flow rate in superheat region; Q_{csp} is the heat transfer rate between the refrigerant and the tube wall in superheat region; A_c is the cross-sectional area of the condenser and L_{c1} is the length of the superheat region.

B. Conservation of mass and energy in two-phase region

Similarly, the mass and energy conservation equations in two-phase region can be calculated respectively by

$$\left(\frac{d\rho_{cf}}{dP_c}(1-\gamma_c)+\frac{d\rho_{cg}}{dP_c}\gamma_c\right)A_cL_{c2}\dot{P}_c+(\rho_{cg}-\rho_{cf})A_c\dot{L}_{c2}\gamma_c+(\rho_{cg}-\rho_{cf})A_c\dot{L}_{c1}+\Delta\dot{m}_{c2}=0 \tag{17}$$

$$\begin{aligned}\left(\frac{d(\rho_{cf}h_{cf})}{dP_c}(1-\gamma_c)+\frac{d(\rho_{cg}h_{cg})}{dP_c}\gamma_c-1\right)&A_cL_{c2}\dot{P}_c+(\rho_{cg}h_{cg}-\rho_{cf}h_{cf})A_c\dot{L}_{c1}+(\rho_{cg}h_{cg}-\rho_{cf}h_{cf})A_c\dot{L}_{c2}\gamma_c\\&+(\Delta\dot{m}_{c2}+\Delta\dot{m}_{c1}+\dot{m}_{ci})h_{cf}-(\Delta\dot{m}_{c1}+\dot{m}_{ci})h_{cg}=Q_{ctp}\end{aligned} \tag{18}$$

where ρ_{c2} and h_{c2} are the refrigerant density and enthalpy in two-phase region, respectively; $\Delta\dot{m}_{c2} = \dot{m}_{z=L_{c2}} - \dot{m}_{z=L_{c1}}$ is the variation of the refrigerant mass flow rate in two-phase region; Q_{ctp} denotes the heat transfer rate between the refrigerant and the tube wall, and L_{c2} is the length of the two-phase region; γ_c is the constant mean void fraction in two-phase region.

C. Conservation of mass and energy in subcool region

Similarly, the resulting mass and energy conservation equations can be written as

$$\left(\frac{\partial\rho_{c3}}{\partial P_c}+\frac{1}{2}\frac{\partial\rho_{c3}}{\partial h_{c3}}\frac{dh_{cf}}{dP_c}\right)A_cL_{c3}\dot{P}_c+\frac{1}{2}\frac{\partial\rho_{c3}}{\partial h_{c3}}A_cL_{c3}\dot{h}_{co}+A_c(\rho_{cf}-\rho_{c3})(\dot{L}_{c1}+\dot{L}_{c2})+\Delta\dot{m}_{c3}=0 \tag{19}$$

$$\begin{aligned}\left(\frac{\partial\rho_{c3}}{\partial P_c}h_{c3}+\frac{1}{2}\left(\frac{\partial\rho_{c3}}{\partial h_{c3}}\frac{d\rho_{cf}}{dP_c}h_{c3}+\frac{dh_{cf}}{dP_c}\rho_{c3}\right)-1\right)&A_cL_{c3}\dot{P}_c+\frac{1}{2}\left(\rho_{c3}+\frac{\partial\rho_{c3}}{\partial h_{c3}}h_{c3}\right)A_cL_{c3}\dot{h}_{co}\\&+A_c(\rho_{cf}h_{cf}-\rho_{c3}h_{c3})(\dot{L}_{c1}+\dot{L}_{c2})+\dot{m}_{co}h_{co}-(\Delta\dot{m}_{c2}+\Delta\dot{m}_{c1}+\dot{m}_{ci})h_{cf}=Q_{csub}\end{aligned} \tag{20}$$

where h_{c3} and ρ_{c3} are the refrigerant enthalpy and density in subcool region, respectively; $\Delta\dot{m}_{c3} = \dot{m}_{z=L_{cT}} - \dot{m}_{z=L_{c2}}$ is the variation of the refrigerant mass flow rate in subcool region; $\dot{m}_{co}$ is the

refrigerant mass flow rate at the condenser outlet; Q_{csub} denotes the heat transfer rate between the refrigerant and the tube wall in this region, and L_{c3} (i.e. $L_{c3} = L_{cT} - L_{c2} - L_{c1}$) is the length of the subcool region; γ_c is the constant mean void fraction in subcool region.

D. Governing ordinary differential equations

From the view of the overall thermal process throughout the condenser, an obviously unique characteristic of the proposed model lies in the following equation

$$\int_0^{L_{cT}} \frac{\partial \dot{m}}{\partial z} dz = \int_0^{L_{c1}} \frac{\partial \dot{m}}{\partial z} dz + \int_{L_{c1}}^{L_{c2}} \frac{\partial \dot{m}}{\partial z} dz + \int_{L_{c2}}^{L_{cT}} \frac{\partial \dot{m}}{\partial z} dz \tag{21}$$

Integrating each term of equation (22), it easily obtains

$$\dot{m}_{co} - \dot{m}_{ci} = \Delta \dot{m}_{c1} + \Delta \dot{m}_{c2} + \Delta \dot{m}_{c3} \tag{22}$$

It is worth noting that the left hand side of equation (22) represents the total of the dynamics of the refrigerant mass flow rate in different fluid phase regions and the right one depicts the variation of the refrigerant mass flow rate through the condenser, rather than describing the dynamics of the refrigerant mass flow rate on the boundary interface.

Based on the above analysis and those equations (15) - (22), the complete dynamic model of the condenser can be presented in a nonlinear state space form shown below:

$$\dot{x}_c = Z_c^{-1}(x_c) f(x_c, u_c) \tag{23}$$

with the system state $x_c = \begin{bmatrix} L_{c1} & L_{c2} & P_c & h_{co} \end{bmatrix}^T$, system input $u_c = \begin{bmatrix} \dot{m}_{ci} & \dot{m}_{co} \end{bmatrix}^T$ and system noise $w_c = \begin{bmatrix} Q_{csp} & Q_{ctp} & Q_{sub} \end{bmatrix}^T$, where $f(x_c, u_c)$ and $Z_c(x_c)$ are obtained from

$$f(x_c, u_c) = \begin{bmatrix} \dot{m}_{ci}\left(h_{ci} - h_{cg}\right) - \left(\frac{1}{2}\frac{\partial \rho_{c1}}{\partial h_{c1}}(h_{c1} - h_{cg}) + \frac{1}{2}\rho_{c1}\right) A_c L_{c1} \dot{h}_{ci} + Q_{csp} \\ \dot{m}_{ci} h_{cg} - \dot{m}_{co} h_{cf} - \frac{1}{2}\frac{\partial \rho_{c1}}{\partial h_{c1}} h_{cg} A_c L_{c1} \dot{h}_{ci} + Q_{ctp} \\ \dot{m}_{co}(h_{cf} - h_{co}) + Q_{csub} \\ \dot{m}_{ci} - \dot{m}_{co} - \frac{1}{2}\frac{\partial \rho_{c1}}{\partial h_{c1}} A_c L_{c1} \dot{h}_{ci} \end{bmatrix}, \quad Z_c(x_c) = \begin{bmatrix} c_{11} & 0 & c_{13} & 0 \\ c_{21} & c_{22} & c_{23} & c_{24} \\ c_{31} & c_{32} & c_{33} & c_{34} \\ c_{41} & c_{42} & c_{43} & c_{44} \end{bmatrix}$$

and the elements of matrix $Z_c(x_c)$ are shown in Table 2 (Appendix B for the calculations of governing ordinary differential equations of the condenser).

Table 2 Elements of matrix $Z_c(x_c)$

c_{11}	$\rho_{c1}(h_{c1}-h_{cg})A_c$
c_{13}	$\left((\frac{\partial\rho_{c1}}{\partial P_c}+\frac{1}{2}\frac{\partial\rho_{c1}}{\partial h_{c1}}\frac{dh_{cg}}{dP_c})(h_{c1}-h_{cg})+\frac{1}{2}\frac{dh_{cg}}{dP_c}\rho_{c1}-1\right)A_cL_{c1}$
c_{21}	$\left(\rho_{c1}h_{cg}-\rho_{c3}h_{cf}\right)A_c$
c_{22}	$\left((\rho_{cg}h_{cg}-\rho_{cf}h_{cf})\gamma_c+(\rho_{cf}-\rho_{c3})h_{cf}\right)A_c$
c_{23}	$\left((\frac{\partial\rho_{c1}}{\partial P_c}+\frac{1}{2}\frac{\partial\rho_{c1}}{\partial h_{c1}}\frac{dh_{cg}}{dP_c})h_{cg}L_{c1}+(\frac{d(\rho_{cf}h_{cf})}{dP_c}(1-\gamma_c)+\frac{d(\rho_{cg}h_{cg})}{dP_c}\gamma_c-1)L_{c2}+(\frac{\partial\rho_{c3}}{\partial P_c}+\frac{1}{2}\frac{\partial\rho_{c3}}{\partial h_{c3}}\frac{dh_{cf}}{dP_c})h_{cf}L_{c3}\right)A_c$
c_{24}	$\frac{1}{2}\frac{\partial\rho_{c3}}{\partial h_{c3}}A_cL_{c3}h_{cf}$
c_{31}	$\rho_{c3}(h_{cf}-h_{c3})A_c$
c_{32}	$\rho_{c3}(h_{cf}-h_{c3})A_c$
c_{33}	$\left((\frac{\partial\rho_{c3}}{\partial P_c}+\frac{1}{2}\frac{\partial\rho_{c3}}{\partial h_{c3}}\frac{dh_{cf}}{dP_c})(h_{c3}-h_{cf})+\frac{1}{2}\frac{dh_{cf}}{dP_c}\rho_{c3}-1\right)A_cL_{c3}$
c_{34}	$\frac{1}{2}\left(\frac{\partial\rho_{c3}}{\partial h_{c3}}\left(h_{c3}-h_{cf}\right)+\rho_{c3}\right)A_cL_{c3}$
c_{41}	$\left(\rho_{c1}-\rho_{c3}\right)A_c$
c_{42}	$\left((\rho_{cg}-\rho_{cf})\gamma_c+(\rho_{cf}-\rho_{c3})\right)A_c$
c_{43}	$\left((\frac{\partial\rho_{c1}}{\partial P_c}+\frac{1}{2}\frac{\partial\rho_{c1}}{\partial h_{c1}}\frac{dh_{cg}}{dP_c})L_{c1}+(\frac{d\rho_{cf}}{dP_c}(1-\gamma_c)+\frac{d\rho_{cg}}{dP_c}\gamma_c)L_{c2}+(\frac{\partial\rho_{c3}}{\partial P_c}+\frac{1}{2}\frac{\partial\rho_{c3}}{\partial h_{c3}}\frac{dh_{cf}}{dP_c})L_{c3}\right)A_c$
c_{44}	$\frac{1}{2}\frac{\partial\rho_{c3}}{\partial h_{c3}}A_cL_{c3}$

As for equations (14) and (23), it is easily seen that much simpler low-order models of the two heat exchangers have been presented based on the dynamic behaviors of the refrigerant mass flow rates in multiple fluid phase regions and the considerations of the heat transfer rates regarded as the measured noises, compared with the dynamic model proposed by [10]. Furthermore, the heat transfer rates w_e and w_c between the refrigerant and the tube wall through the two heat exchangers can be obtained by the following NTU method.

Because evaporator and condenser are the fin-tube counter-flow heat exchangers, these heat transfer rates in fluid phase regions are evaluated by the Number of Transfer Units method [8], which contributes to reduce model order at the cost of the model accuracy and simplify system analysis and control design. Then, heat transfer rate Q in every fluid phase region can be derived from the following equations

$$Q=\varepsilon C_{\min}(T_{h,i}-T_{c,i}) \tag{24}$$

where effectiveness ε is the ratio between the actual heat transfer rate and the maximum feasible heat transfer rate, $T_{h,i} - T_{c,i}$ is the temperature difference between the inlet temperature of the hot stream and that of the cold stream. Heat capacity rate C_h and C_c (i.e. mass flow rate multiplied by specific heat) for hot and cold streams respectively, and the smaller one is denoted as $C_{\min}$. For a given heat exchanger, ε can be calculated based on the heat capacity ratio $C_r = C_{\min} / C_{\max}$ and the number of transfer units $NTU = UA / C_{\min}$, where U is the overall heat transfer coefficient and A is the heat transfer area. Therefore, the effectiveness of a counter-current flow heat exchanger is calculated by

$$\varepsilon = \frac{1-\exp[-NTU(1-C_r)]}{1-C_r \exp[-NTU(1-C_r)]} \qquad (C_r \neq 0,1) \tag{25}$$

Furthermore, it has $\varepsilon = NTU/(1+NTU)$ for $C_r = 1$ and $\varepsilon = 1-\exp(-NTU)$ for $C_r = 0$.

In addition, it is worth noting that under steady state condition, it easily gives $Q_{etp} = \dot{m}_{e1}(h_{eg} - h_{ei})$, $Q_{esp} = \dot{m}_{e2}(h_{eo} - h_{eg})$, $Q_{csp} = \dot{m}_{c1}(h_{cg} - h_{ci})$, $Q_{ctp} = \dot{m}_{c2}(h_{cf} - h_{cg})$ and $Q_{csub} = \dot{m}_{c3}(h_{co} - h_{cf})$ when refrigerant mass flow rates, pressures and enthalpies in different fluid phase regions can be considered as constants.

3.2. Static model of other components

Due to the dynamic behaviours of the compressor, electrical expansion valve and ejector varying much faster than that of the heat exchangers in the refrigeration system, these components should be modelled into a static form [9, 10].

3.2.1. Compressor

The variable speed compressor can provide the refrigerant mass flow rate

$$\dot{m}_{vsc} = \omega_{vsc} \rho_{vsc,in} V_{vsc} \eta_V = \dot{m}_{eo} \tag{26}$$

where $\dot{m}_{vsc}$ is the mass flow rate through compressor, ω_{vsc} is the compressor speed, $\rho_{vsc,in}$ is the refrigerant density at the inlet, V_{vsc} is the displaced volume of the compressor, and η_V is its volumetric efficiency denoting the ratio of induced gas volume to the discharged gas volume. The term $\rho_{vsc} V_{vsc} \eta_V$ characterizes the compressor capacity, where η_V can be modeled by

$$\eta_V = \left(1 + B_{vsc,1} + B_{vsc,2} \left(\frac{P_{vsc,out}}{P_{vsc,in}} \right)^{1/n} \right) \tag{27}$$

where $B_{vsc,1}$ and $B_{vsc,2}$ are volumetric efficiency coefficients for the compressor identified by the nonlinear least square method [1], $P_{vsc,in}$ and $P_{vsc,out}$ are inlet and outlet pressures, and n is the polytropic coefficient. Furthermore, compression is always assumed to an adiabatic process with an isentropic efficiency η_{vsc}, so the refrigerant enthalpy at the compressor outlet can be calculated by

$$h_{vsc,out} = \frac{h_{vsc,outs} - h_{vsc,in}}{\eta_{vsc}} + h_{vsc,in} \tag{28}$$

where $h_{vsc,outs} = h(s_{in},\ P_{vsc,out})$ and $s_{in} = s(P_{vsc,in}, h_{vsc,in})$ are the enthalpy at the exit assuming an isentropic compression process and the entropy at the inlet, $h_{vsc,in}$ is the enthalpy at inlet, and $h_{vsc,out}$ is the actual enthalpy at the outlet of the compressor, respectively. The isentropic efficiency of the compression process can be described with the following equation:

$$\eta_{vsc} = d_{vsc,0} + d_{vsc,1}\frac{1}{\omega_{vsc}} + d_{vsc,2}\frac{P_{vsc,out}}{P_{vsc.in}} + d_{vsc,3}\frac{1}{P_{vsc.in}} + d_{vsc,4}\frac{1}{\dot{m}_{vsc}} + d_{vsc,5}(\rho_{vsc,in} - \rho_{sat}) \tag{29}$$

and η_{vsc} can be used to fit and predict the experiment data, where the coefficients $d_{vsc,0}, d_{vsc,1}, d_{vsc,2}, d_{vsc,3}, d_{vsc,4}$ and $d_{vsc,5}$ can be identified by the least square method from the historical experiment data or product manuals. More details may be found in [18].

In addition, compressor power consumption can be evaluated as:

$$W_{vsc} = \frac{\dot{m}_{vsc}(h_{vsc,out} - h_{vsc,in})}{\eta_{com}} \tag{30}$$

where η_{com} is the delivery efficiency accounting for all capacity losses, also obtained from the system identification exercise.

3.2.2. Electrical expansion valve (EEV)

The expansion valve is considered as an isenthalpic process with the same enthalpy at inlet and outlet. The mass flow rate of expansion valve deciding on valve opening percentage, pressure difference and inlet refrigerant density can be derived from the orifice equation:

$$\begin{aligned} \dot{m}_{eev} &= (d_{eev,1} + d_{eev,2}A_{eev})\sqrt{\rho_{eev}(P_c - P_e)} \\ \dot{m}_{eev} &= \dot{m}_{ei} = \dot{m}_{co} \end{aligned} \tag{31}$$

where $\dot{m}_{eev}$ is the mass flow rate of the refrigerant through the expansion valve, $d_{eev,1}$ and $d_{eev,2}$ are the discharge coefficients determined by correlations developed specifically in relevant literatures, A_{eev} is the

effective flow area, ρ_{eev} is the refrigerant density at valve inlet, $(P_c - P_e)$ is the refrigerant pressure difference between the valve inlet and outlet.

3.2.3. Ejector

The ejector is the important component for the ejector system as shown in Fig. 3. In this paper, the ejector performance analysis can be carried out based on the 1D model developed by [5], rather than using the CFD model [3, 19]. To simplify the modelling problem, some assumptions should be made:

1) Fluid through the ejector is steady and one-dimensional.
2) Gas through the ejector behaves as ideal and has constant specific heat ratio.
3) Velocities of the two fluids at the inlet and outlet of the ejector are negligible.
4) Two fluids begin to mix with a uniform pressure, i.e. $P_{p2} = P_{s2}$, when the secondary flow reaches choking condition at section 2.
5) The ejector is adiabatic.

Based on the above assumptions, the following governing equations can be further derived.

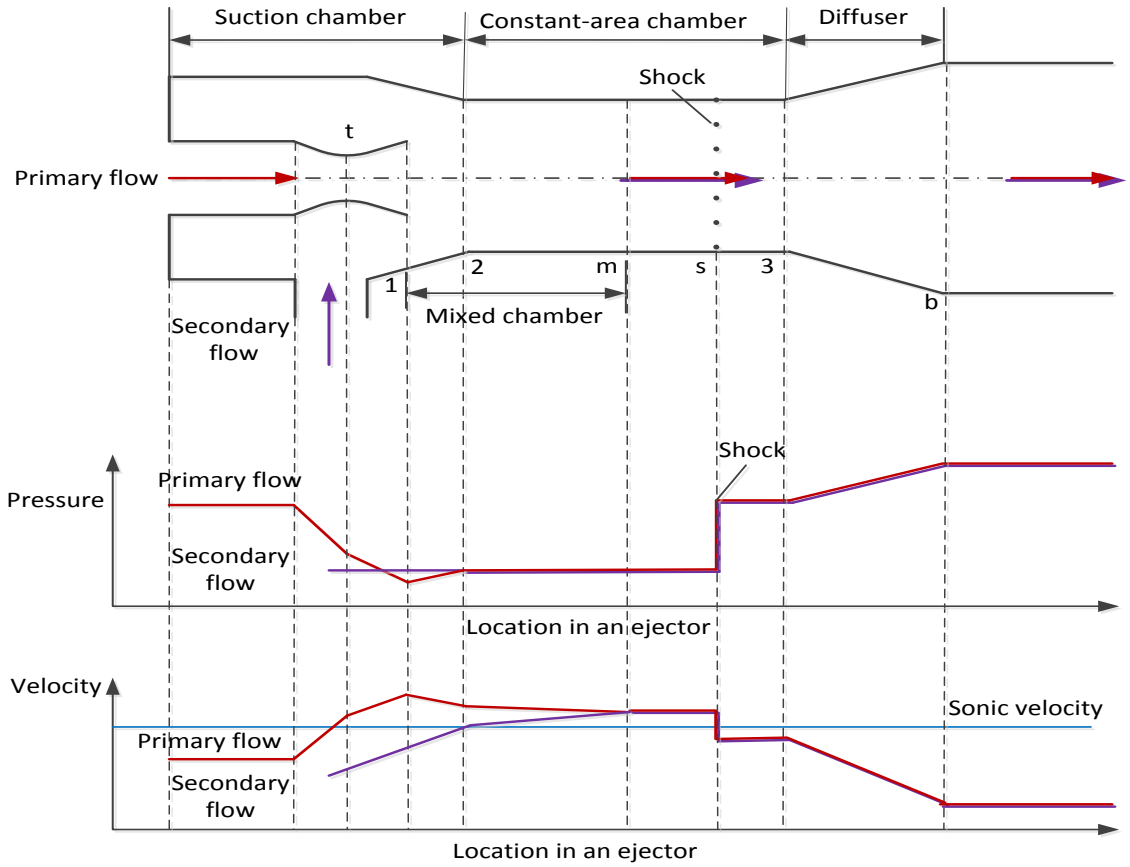

Fig. 3. Diagram of the pressure and velocity distribution in the ejector

A. Primary flow in the nozzle

In the converging-diverging nozzle, based on the ejector structure and the fluid thermodynamic properties, the mass flow rate of the primary flow through the nozzle at choking condition can be obtained using the isentropic flow relation

$$\dot{m}_p = P_p A_t \left(\frac{\gamma \eta_p}{R_g T_p}\right)^{\frac{1}{2}} \left(\frac{2}{\gamma+1}\right)^{\frac{\gamma+1}{2(\gamma-1)}} \tag{32}$$

where η_p represents the isentropic efficiency of the flow at the nozzle, P_p and T_p are the pressure and temperature of the primary flow at the nozzle, respectively. Furthermore, the relationships between nozzle exit cross-section area A_{p1}, nozzle throat cross-section area A_t, Mach number M_{p1} and pressure P_{p1} at the nozzle exit are expressed by

$$\frac{A_{p1}}{A_t} = \frac{1}{M_{p1}} \left(\frac{2+(\gamma-1)M_{p1}^2}{\gamma+1} \right)^{\frac{\gamma+1}{2(\gamma-1)}} \tag{33}$$

$$\frac{P_p}{P_{p1}} = \left(1+\frac{(\gamma-1)}{2} M_{p1}^2\right)^{\frac{\gamma}{\gamma-1}} \tag{34}$$

B. Primary flow from section 1 to section 2

Before starting to mix with the entrained flow, the primary flow between section 1 and 2 can be approximated with isentropic relations, and then the Mach number M_{p2} of the primary flow at section 2 is derived from

$$\frac{P_{p2}}{P_{p1}} = \left(\frac{2+(\gamma-1)M_{p1}^2}{2+(\gamma-1)M_{p2}^2} \right)^{\frac{\gamma}{\gamma-1}} \tag{35}$$

Furthermore, effective area of the primary flow at section 2, A_{p2}, is derived from the following equation:

$$\frac{A_{p2}}{A_{p1}} = \frac{\phi_p M_{p1}}{M_{p2}} \left(\frac{2+(\gamma-1)M_{p2}^2}{2+(\gamma-1)M_{p1}^2} \right)^{\frac{\gamma+1}{2(\gamma-1)}} \tag{36}$$

where the isentropic efficiency coefficient ϕ_p represents the losses of primary flow between section 1 and section 2. Furthermore, the temperature of the primary flow at section 2 follows

$$\frac{T_p}{T_{p2}} = 1+\frac{(\gamma-1)M_{p2}^2}{2} \tag{37}$$

C. Entrained flow from ejector inlet to section 2

The dynamic characteristics of the secondary flow through the ejector are much more complicated than those of the primary flow. Under this condition that the secondary flow chokes at section 2, the Mach number of the secondary flow at section 2 can be equal to one, i.e. $M_{s2}=1$. The relationship between the pressure P_s of the secondary flow through the nozzle and its pressure P_{s2} reaching choking condition at section 2 is derived from

$$\frac{P_s}{P_{s2}}=\left(\frac{2+(\gamma-1)M_{s2}^2}{2}\right)^{\frac{\gamma}{\gamma-1}} \tag{38}$$

and the entrained mass flow rate entering the nozzle is calculated by:

$$\dot{m}_s=P_s A_{s2}\sqrt{\frac{\gamma\eta_s}{R_g T_s}}\left(\frac{2}{\gamma+1}\right)^{\frac{\gamma+1}{2(\gamma-1)}} \tag{39}$$

where η_s and T_s are the isentropic efficiency coefficient and temperature of the secondary flow through the nozzle, respectively. However, it is worth noting that $\dot{m}_s=\dot{m}_{vsc}$ for the ejector, and $\dot{m}_{ci}=\dot{m}_s+\dot{m}_p$ for the condenser. Therefore, combining equations (26), (32) and (39), the entrainment ratio can be calculated from the following equation:

$$\omega=\frac{\dot{m}_s}{\dot{m}_p}=\frac{\dot{m}_{vsc}}{\dot{m}_p} \tag{40}$$

In addition, the geometrical cross-section area A_2 at section 2 is the sum of the effective areas of the primary and secondary flows. That is

$$A_2=A_{p2}+A_{s2} \tag{41}$$

where A_{p2} and A_{s2} are the effective areas for the primary and secondary flow at section 2, respectively. The effective area A_{s2} can be solely derived from equations (26) and (39), rather than iterative calculation. Moreover, the temperature and the Mach number M_{s2} of the secondary flow at section 2 follows

$$\frac{T_s}{T_{s2}}=1+\frac{(\gamma-1)M_{s2}^2}{2} \tag{42}$$

D. Two streams in mixed chamber before shock

Two fluids begin to mix after section 2, and mixing process occurs at constant pressure, thus $P_m=P_{p2}=P_{s2}$. Hence, considering the momentum and energy balance between sections 2 and m gives

$$\phi_m(\dot{m}_p v_{p2} + \dot{m}_s v_{s2}) = (\dot{m}_p + \dot{m}_s) v_m \tag{43}$$

$$\dot{m}_p(C_p T_{p2} + \frac{v_{p2}^2}{2}) + \dot{m}_s(C_p T_{s2} + \frac{v_{s2}^2}{2}) = (\dot{m}_p + \dot{m}_s)(C_p T_m + \frac{v_m^2}{2}) \tag{44}$$

where ϕ_m is the mixing efficient coefficient due to the frictional loss and v_m is the velocity of the mixed flow at section m. v_{p2} and v_{s2} are the gas velocity of the primary and entrained flow at section 2, derived by

$$v_{p2} = M_{p2}\sqrt{\gamma R T_{p2}}, \quad v_{s2} = M_{s2}\sqrt{\gamma R T_{s2}} \tag{45}$$

and Mach number M_m of the mixed flow is derived from

$$v_m = M_m \sqrt{\gamma R T_m} \tag{46}$$

E. Mixed flow across the shock from section 2 to section s

A normal shock occurs at section s with a sharp pressure rise, and the mixed flow after the shock undergoes an isentropic process, when the mixed flow between sections m and 3 has a uniform pressure P_3. Then, the gas dynamic relations are

$$\frac{P_3}{P_m} = 1 + \frac{2\gamma}{\gamma + 1}(M_m^2 - 1) \tag{47}$$

$$M_3 = \frac{2 + (\gamma - 1)M_m^2}{2\gamma M_m^2 - (\gamma - 1)} \tag{48}$$

F. Mixed flow through diffuser

The subsonic mixed flow is further compressed in the diffuser. By defining an isentropic efficiency, the back pressure $P_b = P_c$ at the diffuser outlet is obtained as follows:

$$\frac{P_b}{P_3} = \left(\frac{(\gamma - 1)\eta_b M_3^2}{2} + 1 \right) \tag{49}$$

where η_b is the isentropic efficient coefficient of the diffuser.

Referring to Fig. 3, the relationship between the pressure P_s of the secondary flow at the nozzle inlet and the mixed flow P_b at ejector outlet calculated by equations (34) – (49) can be written as

$$P_s = \frac{P_s}{P_m} \cdot \frac{P_m}{P_3} \cdot \frac{P_3}{P_b} \cdot P_b \tag{50}$$

It can be seen that equation (50) builds up the relationship between P_s and P_b. Furthermore, the secondary flow pressure P_s can be derived by solving equation (50) when back pressure $P_b = P_c$ is known.

3.3. Dynamic model of the whole refrigeration system

Much different from a 11th order state space representation of the vapour compression refrigeration cycle proposed by [11], dynamics of the ejector-based refrigeration system can be simply characterized with certain accuracy by 7 system states, 2 system inputs and 5 noises as

$$\begin{bmatrix} Z_e(x_e) & 0 \\ 0 & Z_c(x_c) \end{bmatrix} \begin{bmatrix} \dot{L}_{e1} \\ \dot{P}_e \\ \dot{h}_{eo} \\ \dot{L}_{c1} \\ \dot{L}_{c2} \\ \dot{P}_c \\ \dot{h}_{co} \end{bmatrix} = \begin{bmatrix} \dot{m}_{eev}(h_{ei} - h_{eg}) + Q_{etp} \\ \dot{m}_{vsc}(h_{eg} - h_{eo}) + Q_{esp} \\ \dot{m}_{eev} - \dot{m}_{vsc} \\ (\dot{m}_p + \dot{m}_{vsc})\left(h_{ci} - h_{cg}\right) - \left(\frac{1}{2}\frac{\partial \rho_{c1}}{\partial h_{c1}}(h_{c1} - h_{cg}) + \frac{1}{2}\rho_{c1}\right) A_c L_{c1} \dot{h}_{ci} + Q_{csp} \\ (\dot{m}_p + \dot{m}_{vsc}) h_{cg} - (\dot{m}_p + \dot{m}_{eev}) h_{cf} - \frac{1}{2}\frac{\partial \rho_{c1}}{\partial h_{c1}} h_{cg} A_c L_{c1} \dot{h}_{ci} + Q_{ctp} \\ (\dot{m}_p + \dot{m}_{eev})(h_{cf} - h_{co}) + Q_{csub} \\ (\dot{m}_p + \dot{m}_{vsc}) - (\dot{m}_p + \dot{m}_{eev}) - \frac{1}{2}\frac{\partial \rho_{c1}}{\partial h_{c1}} A_c L_{c1} \dot{h}_{ci} \end{bmatrix} \tag{51}$$

$$y = \begin{bmatrix} P_e \\ P_c \\ P_s \\ SH \end{bmatrix} = \begin{bmatrix} P_e \\ P_c \\ \frac{P_s}{P_m} \cdot \frac{P_m}{P_3} \cdot \frac{P_3}{P_c} \cdot P_c \\ T(P_e, h_{eo}) - T_{sat}(P_e) \end{bmatrix} \tag{52}$$

where $x = [x_e \quad x_c]^T$, $u = [\omega_{vsc} \quad A_v]^T$, $w = [w_e \quad w_c]^T$, and the fluid temperatures in different phase regions are dependent on the pressures and enthalpies except that the saturated temperature is only a function of pressure or temperature.

In the overall ejector refrigeration system, some variables including evaporating pressure P_e, condensing pressure P_c, superheat SH at the evaporator exit and the secondary flow pressure P_s are selected as the controlled variables, which can be regulated to the desire values by some manipulated variables such as the compressor speed and EEV opening. Other variables such as compressor power consumption W_{vsc} and outlet enthalpy $h_{vsc,out}$ are calculated by static functions of the dynamic states. Compared with the model [10], it has some advantages such as lower model order and less computation burden which are beneficial for the real-time control requirement. Though, modelling accuracy will be decreased by using NTU method,

satisfactory system performances still have been obtained by employing the advanced control methods [8, 10, 16] such as robust control, MPC and LQG.

4. Experimental setup

Fig. 4 Photograph of the ejector refrigeration system

In order to validate the proposed model, an experimental rig on the ejector refrigeration system shown in Fig. 4 has been built in Process Instrumentation Laboratory of Nanyang Technological University of Singapore. The corresponding schematic diagram is given in Fig. 5 where several sensor locations for study are equipped. The experimental rig consists of the following components:

- A heater with a maximum power of 6 kW is set at the bottom of a heat transfer oil tank as the heat source of the generator, which keeps the primary flow temperature varying from 90 ℃ to 115 ℃.
- An air-cooling condenser accompanied by a liquid receiver has a maximum condensing load of 10kW, where the condensing temperature ranges from 35 ℃ to 40 ℃.
- Heated by a variable electric heater with a maximum power of 3kW, a hot water tank with temperature varying between 30 ℃ and 34 ℃ is known as an evaporator accompanied by an accumulator, which has certain cooling capacity.

- A compressor with model number XB075Z24 is used, the rotational speed of which changing from 2000rpm to 3700rpm can be regulated by an inverter.
- An electronic expansion valve driven by a step motor is used for regulating the mass flow rate of the refrigerant.

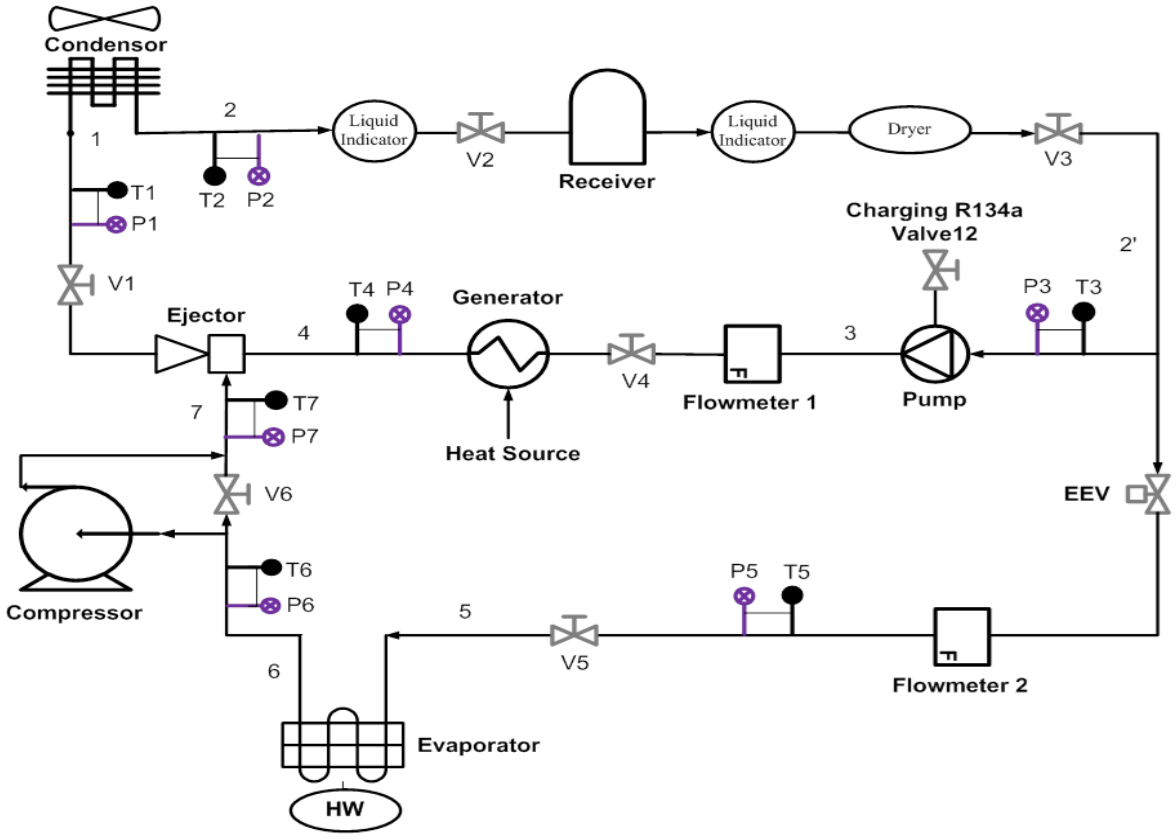

Fig. 5 Schematic diagram of the test rig

In addition, related data acquisitions and control algorithms are developed based on National Instruments Labview 8.6, and the high-temperature and low-temperature devices are properly insulated by foam rubber to reduce heat losses. As shown in Fig. 5, a receiver situated at the outlet of the condenser is used for storing the liquid refrigerant at state '2' and the dryer is used for eliminating the mixed water. Therefore, the modeling part of the receiver and accumulator could be neglected in this work, however superheat and subcooled issues must be considered in the subsequent control design. To measure the operating parameter of refrigerant, some types of temperature and pressure sensors are also set in the system.

- Temperature sensors of PT1000 platinum resistance with error of ±0.3 ℃;
- Pressure transmitters with error of 0.5%;
- Rotor flow meters measuring the mass flow rates of the refrigerant, calibrated with error of ±1.6%.

Accordingly, some important ejector geometry parameters depicted in Table 3 are given as follows:

Table 3 Ejector geometry parameters

Sections	Dimensions	Units
Nozzle diameter Dt	1.6	mm
Nozzle exit diameter D1	2.3	mm
Constant are section diameter Dm	3.4	mm
Nozzle exit position to constant area section inlet NXP	5.0	mm
Constant area section length Lm	20.0	mm
Diffuser length Ld	70.0	mm
Nozzle convergent section length Lc,n	34.0	mm
Nozzle divergent section length Ld,n	4.0	mm

5. Results and discussion

The refrigerant R134a can be chosen as working fluid because of its international recognition for no bad effects against ozonosphere and excellent safety performances such as nontoxic, nonexplosive and uninflammable. However, R134a is going to be banned within several countries, due to its high Global Warming Potential (GWP=1300). Thermodynamics properties of working fluid R134a are obtained from software REFPROP 7.0 developed by the National Institute of Standards and Technology of the United States [20].

Table 4 Range of the operating conditions

Variables	Range	Units
Evaporating pressure	2.5-4.5	bar
Condensing pressure	9-10	bar
Primary flow pressure	15-25	bar
Secondary flow pressure	5-8	bar
Evaporating temperature	-4-13	℃
Condensing temperature	35-40	℃
Compressor speed	2000-3700	rpm
EEV opening	60%-100%	-
Refrigerant mass flow rate	0.003-0.04	kg/s
Air inlet temperature through condenser	30-36	℃
Air outlet temperature through condenser	36-42	℃
Air mass flow rate through condenser	0.1-1.0	kg/s

The experimental tests are carried out under different operating conditions through changing related parameters of R134a and the secondary fluid. Table 4 lists the operating range of the ejector refrigeration cycle for this model validation. The condenser pressure, evaporator pressure, superheat and subcool are the regulated system outputs. The compressor speed and EEV opening are the controllable inputs, while the condenser fan and the pump are used for regulating the air and refrigerant speed.

For error analysis, predicted results are compared with obtained experimental results. Four types of error descriptions including the relative error (RE), the root mean square error (RSE), the standard deviation (SD) and the coefficient of variance (CV) are adopted to point out how the proposed model fits the experimental data. These definitions [21] can be given in the form of equations as follows:

$$\mathrm{RE} = \frac{\sum_{i=1}^{N} \left| z_{cal,i} - z_{data,i} \right| / z_{data,i}}{N} \times 100\% \tag{53}$$

$$\mathrm{RSE} = \sqrt{\frac{\sum_{i=1}^{N} (z_{cal,i} - z_{data,i})^2}{N}} \tag{54}$$

$$\mathrm{SD} = \sqrt{\frac{\sum_{i=1}^{N} (z_{data,i} - z_{data,ave})^2}{N}} \tag{55}$$

$$\mathrm{CV} = \frac{\mathrm{RMSE}}{z_{data,ave}} \times 100\% \tag{56}$$

where $z_{cal,i}$ and $z_{data,i}$ are the calculated and experimental values for a set of N samples, respectively. $z_{data,ave} = \frac{1}{N}\sum_{i=1}^{N} z_{data,i}$ is the average value of the experimental data.

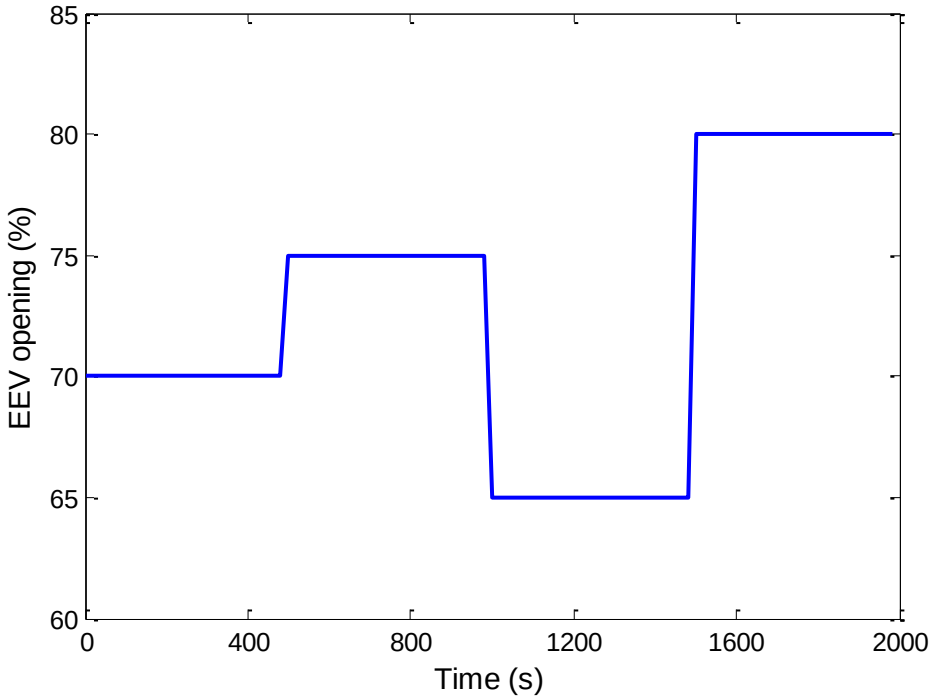

Fig.6. Changes of EEV opening

To verify the accuracy of the proposed model in predicting the dynamical behavior, four system variables including evaporating pressure, refrigerant enthalpy at the evaporator outlet, condensing pressure

and refrigerant enthalpy at the condenser outlet are tested in a wide range of operating conditions. Fig. 6 shows the step changes of the EEV opening considered as a control input variable. In spite of the step changes of the EEV opening, predicted results of all validations can be found to have a good match with the experimental results, as shown in Figs. 7–10, respectively.

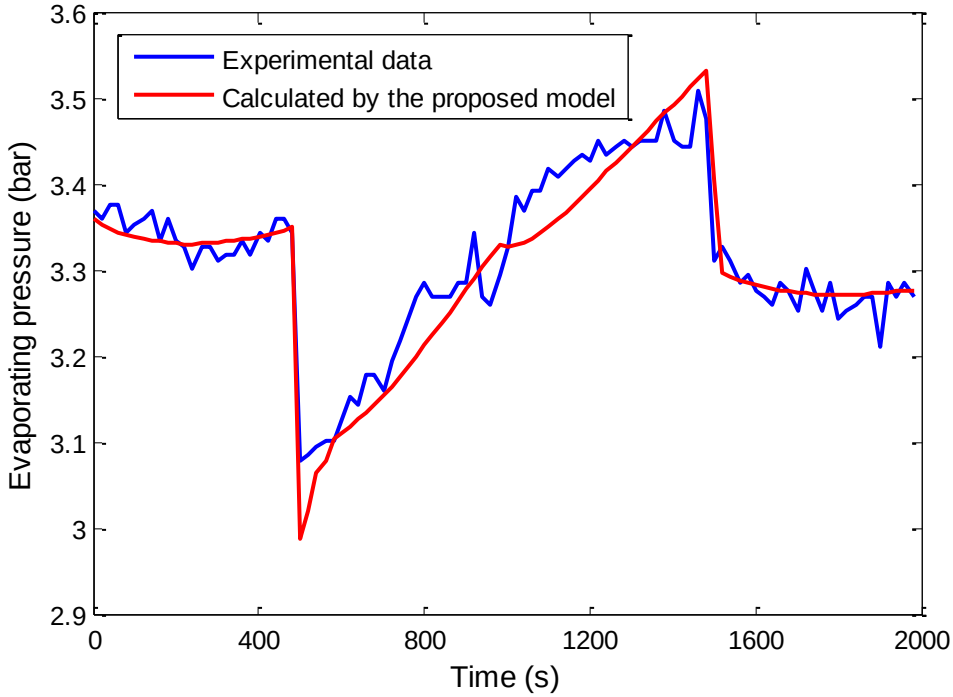

Fig.7. Calculated and experimental evaporating pressure

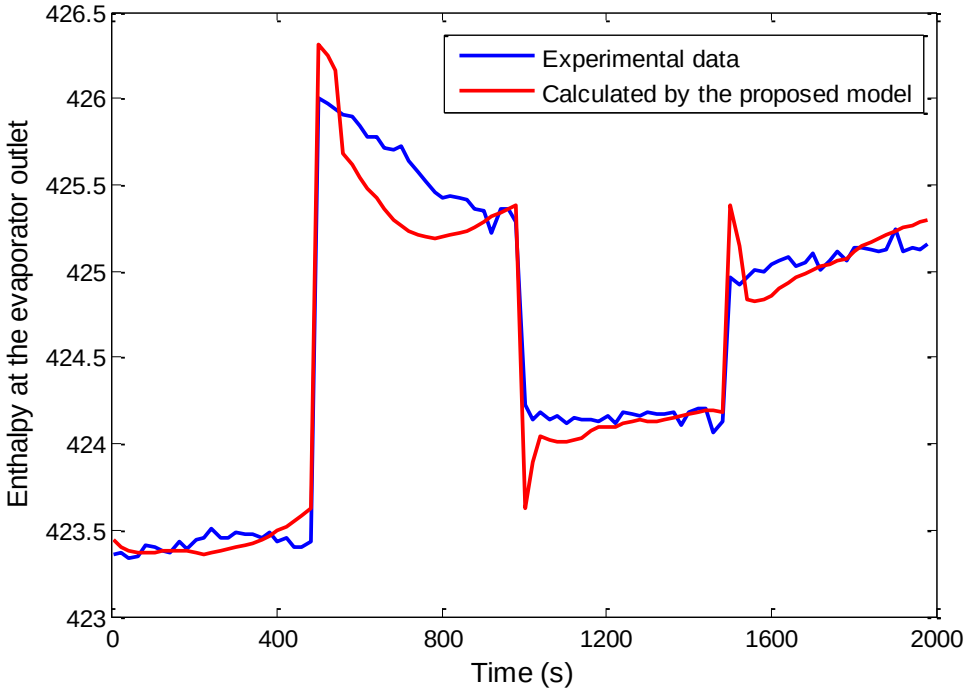

Fig.8. Calculated and experimental refrigerant enthalpy at the evaporator outlet

Fig. 7 displays the dynamical response of the evaporating pressure with respect to the variation test of EEV opening. The comparison between the measured and calculated evaporating pressure indicates that the proposed model can describe the dynamics of the evaporating pressure with a high degree of accuracy, except that there are large fluctuations with the transient changes of the EEV opening. The largest error between the measured and calculated evaporating pressure occurs around at time instant 600 s. Fig. 8 shows the plots of the calculated and experimental values of the refrigerant enthalpy leaving the evaporator, caused by the step changes of the EEV opening. During this time from 500 s to 1000 s, the experimental values of the refrigerant enthalpy slightly deviate from the predicted values. Nevertheless, from the view of the overall comparison results, Fig. 8 still shows the good agreement between the calculated and experimental values, which means that the proposed model can accurately evaluate the behavior of the refrigerant enthalpy at the evaporator outlet.

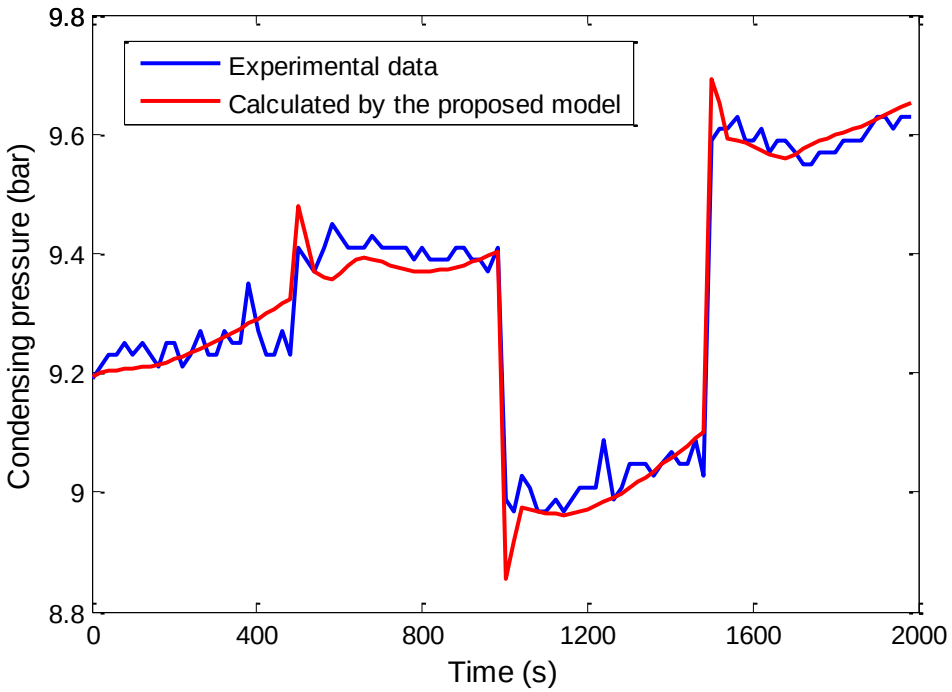

Fig.9. Calculated and experimental condensing pressure

Moreover, Fig. 9 depicts the comparison of the calculated and measured results for the condensing pressure. The tendency of the calculated result is approximately close to that obtained from experimental data, except that there is a larger error between the calculated and measured values when the value of the EEV opening instantaneously changes each time. Finally, Fig. 10 presents the evolution of the refrigerant enthalpy leaving the condenser. It can be easily seen from this figure that although a calculated value of the refrigerant enthalpy having the largest deviation from its experimental value occurs at time instant 800 s, most of the values of the refrigerant enthalpy calculated by the proposed model can be basically in good

agreement with the experiment values. Based on the above experimental results shown in Figs. 6–10, the proposed model has a good dynamical performance in evaluating the behavior of the refrigeration system, which can prepare for the controller design and real-time optimization in future.

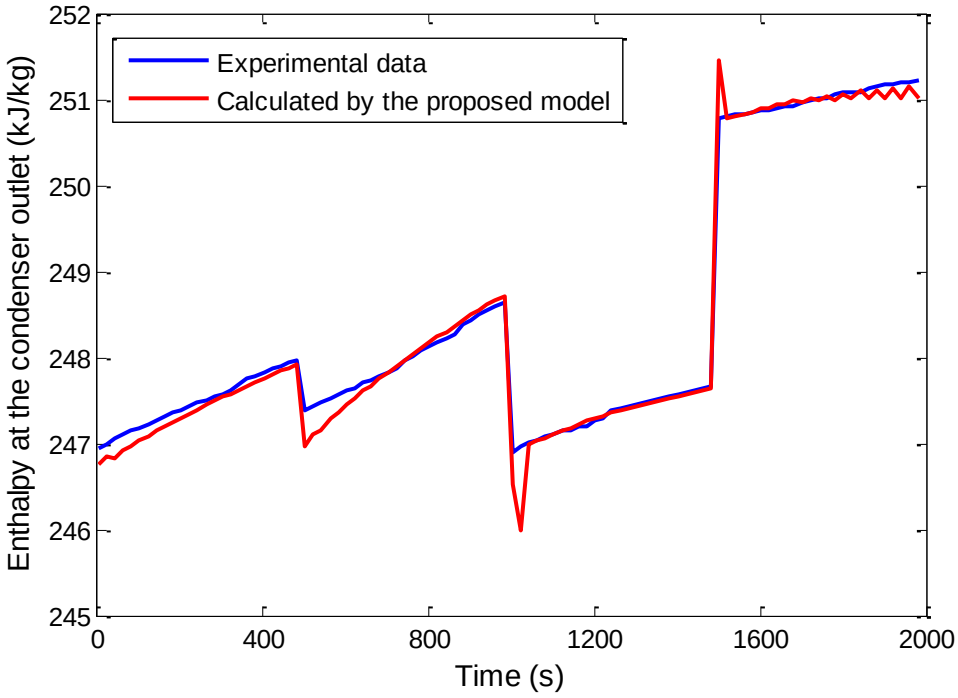

Fig.10. Calculated and experimental refrigerant enthalpy at the condenser outlet

In addition, Table 5 shows several statistical characteristics of four error descriptions for four system parameters. It can be noted that the error results of the proposed model are relatively small. The causes for the small error results exist in three factors: (1) high accuracy of experimental data due to the smaller measurement errors of the sensors, (2) the precise calculation of fluid properties obtained from software REFPROP 7.0 and (3) the availability of the proposed model.

Table 5 Statistic characteristics of the four system parameters

parameter	$z_{data,ave}$	RSE	RE (%)	SD	CV (%)
P_e	3.32	0.04	0.27	0.10	1.02
h_{eo}	424.57	0.21	0.02	0.85	0.05
P_c	9.32	0.04	0.34	0.22	0.43
h_{co}	248.45	0.16	0.03	1.52	0.07

It worth noting that heat transfer rate Q_e at evaporator considered as the disturbance variable has an important effect on the proposed dynamic model described by equation (51), and then the experimental

results of Q_e is given in Fig. 11. Closely related to Q_e, compressor power W_{vsc}, heat transfer rate Q_e at evaporator and heat transfer rate $Q_{generator}$ at generator are also given in Fig. 11. From this figure, the variation tendency of W_{vsc} described by the equation (30) is a bit similar with the change of the EEV opening. However, Q_e depending on the ambient environment, the heat transfer area and the refrigerant is contrary to the variation tendency of W_{vsc}. With the change of Q_e and EEV opening, other experimental results are shown respectively in the above Figs 6-9. Very larger than the value of W_{vsc} and Q_e, the value of $Q_{generator}$ with the maximum value 6 kW at generator changes between 4.7kW and 6 kW, which indicates that a large number of low grade energy from waste heat can be used for recycling and reusing.

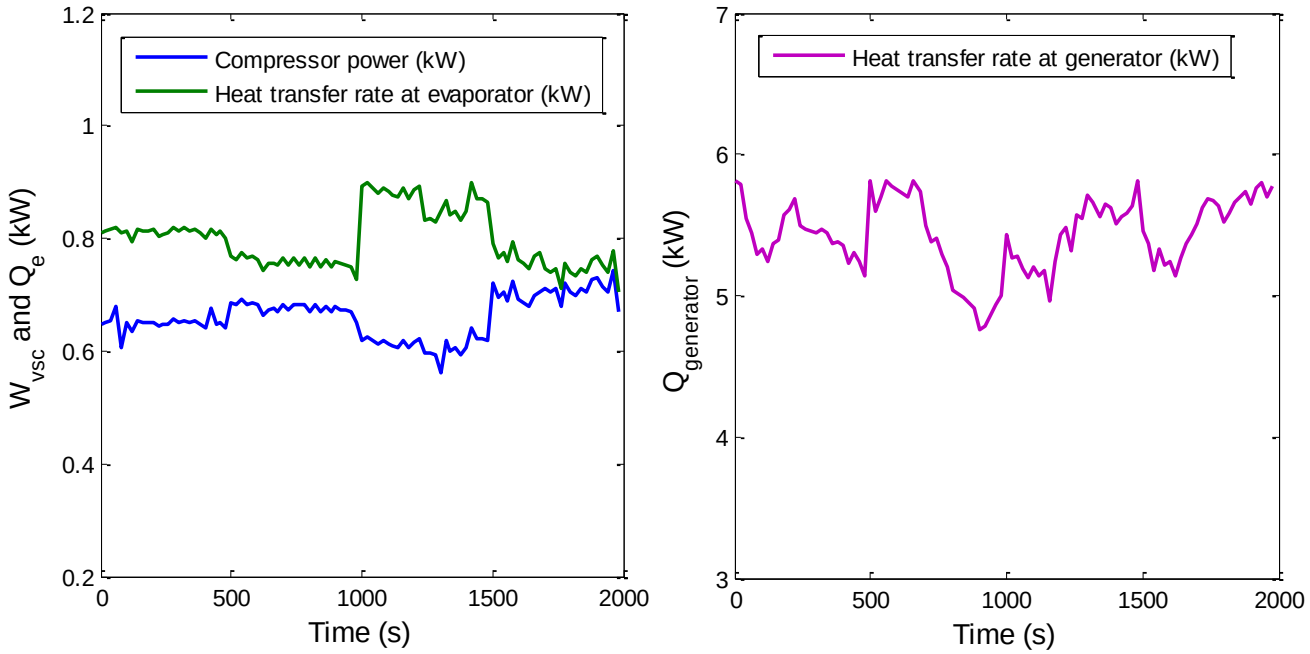

Fig.11. Compressor power, heat transfer rates at evaporator and generator

6. Conclusions

A global low-order state-space model was developed for the ejector-based refrigeration system, based on the first principle of the mass and energy conservation. Compared with the existing methods, the NTU method was applied to evaluate the heat transfer rate between the refrigerant and the tube wall in multiple fluid phase regions of the heat exchangers to obtain the reduced-order models of the evaporator and the condenser respectively. Furthermore, a 1D static model of the ejector proposed by [5] can be used to predict the ejector performance at critical and subcritical operating condition. Real time data from experimental testing can be used to clarify the validity of the proposed model. Meanwhile, the experimental results gave a good match to the real-time experimental data over the whole operation range. In addition, the performance

optimization problem of the ejector-based refrigeration system including cooling capacity and energy efficiency such as COP will be focused on in the future.

Nomenclature

A	area, m^2
B	coefficient
C_p	specific heat capacity at constant pressure, kJ/(kg ·K)
M	March number
P	pressure, bar
Q	heat transfer rate, kW
$\dot{Q}$	derivative of heat transfer rate, kW/s
R_g	gas constant, kJ/(kg ·K)
T	temperature, ℃
V	displacement volume, m^3
W	work, kW
d	coefficient
h	enthalpy, kJ/kg
$\dot{m}$	mass flow rate, kg/s
$\Delta\dot{m}$	variation of the mass flow rate, kg/s
v	gas velocity, g/s
w	noise
ϕ	coefficient
γ	mean void fraction or specific heat ratio of gas
η	efficiency
ρ	density, kg/m^3
ω	compressor speed, rpm

Subscripts

b	exit of ejector
c	condenser
e	evaporator
eev	electrical expansion valve
g	gas
i	in
m	mixed flow
o	out
p	primary flow
s	suction or secondary flow
t	nozzle throat
vsc	varying speed compressor
w	tube wall of heat exchanger
y	location of choking for the secondary flow
1	nozzle exit

2 entrance of the constant-area section
3 exit of the constant-area section

Appendix A. Calculations of partial differential equations in superheat region of the evaporator

Based on equations (1) and (2), partial differential equations for refrigerant mass and energy in superheat region are given by

$$\frac{\partial(\rho_{e2}A_e)}{\partial t}+\frac{\partial \dot{m}}{\partial z}=0 \tag{A1}$$

$$\frac{\partial(\rho_{e2}A_e h_{e2}-A_e P_e)}{\partial t}+\frac{\partial\left(\dot{m}h_{e2}\right)}{\partial z}=\frac{\partial Q_{esp}}{\partial z} \tag{A2}$$

In the superheat region, the refrigerant enthalpy h_{e2} can be assumed to be an average of the refrigerant saturated vapour and outlet enthalpies h_{eg} and h_{eo} as $h_{e2}=0.5(h_{eg}+h_{eo})$, and then the density of the refrigerant is described as a function of pressure P_e and enthalpy h_{e2} as $\rho_{e2}=\rho(P_e,h_{e2})$. Therefore, time derivative of refrigerant density and enthalpy can be calculated by

$$\dot{\rho}_{e2}=\frac{\partial\rho_{e2}}{\partial P_e}\dot{P}_e+\frac{\partial\rho_{e2}}{\partial h_{e2}}\dot{h}_{e2} \tag{A3}$$

Applying Leibniz's rules and integrating each term of equation (A1) from L_{e1} to L_{eT} (i.e. $L_{e2}=L_{eT}-L_{e1}$) in the superheat region, this equation (7) is easily derived through equations (A1) and (A3).

Furthermore, by integrating the equation (A2) over the length L_{e2} of the superheat region and applying the Leibniz's rule, the first term on the left side of the equations (A2) becomes

$$\begin{aligned}\int_{L_{e1}}^{L_{eT}}\frac{\partial(\rho_{e2}A_e h_{e2}-A_e P_e)}{\partial t}dz=&\left((\frac{\partial\rho_{e2}}{\partial P_e}+\frac{1}{2}\frac{\partial\rho_{e2}}{\partial h_{e2}}\frac{dh_{eg}}{dP_e})h_{e2}+\frac{1}{2}\frac{dh_{eg}}{dP_e}\rho_{e2}-1\right)A_e L_{e2}\dot{P}_e\\&+\frac{1}{2}\left(\frac{\partial\rho_{e2}}{\partial h_{e2}}h_{e2}+\rho_{e2}\right)A_e L_{e2}\dot{h}_{eo}+(\rho_{eg}h_{eg}-\rho_{e2}h_{e2})\dot{L}_{e1}\end{aligned} \tag{A4}$$

Integrating the rest of the equation (A2) results in

$$\int_{L_{e1}}^{L_{eT}}\left(\frac{\partial\left(\dot{m}h_{e2}-Q_{esp}\right)}{\partial z}\right)dz=\dot{m}_{eo}h_{eo}-(\dot{m}_{eo}-\Delta\dot{m}_{e2})h_{eg}-Q_{esp} \tag{A5}$$

Combing the results (A4) - (A5) of the integration, the equation (8) can be obtained.

Appendix B. Calculations of governing ordinary differential equations of the condenser

Solving for the intermediate mass flow rates in multiple fluid phase regions, the following equations can be obtained:

$$\Delta\dot{m}_{c1} = -\left(\frac{\partial\rho_{c1}}{\partial P_c} + \frac{1}{2}\frac{\partial\rho_{c1}}{\partial h_{c1}}\frac{dh_{cg}}{dP_c}\right)A_c L_{c1}\dot{P}_c - \frac{1}{2}\frac{\partial\rho_{c1}}{\partial h_{c1}}A_c L_{c1}\dot{h}_{ci} - (\rho_{c1}-\rho_{cg})A_c\dot{L}_{c1} \tag{B1}$$

$$\Delta\dot{m}_{c2} = -\left(\frac{d\rho_{cf}}{dP_c}(1-\gamma_c) + \frac{d\rho_{cg}}{dP_c}\gamma_c\right)A_c L_{c2}\dot{P}_c - (\rho_{cg}-\rho_{cf})A_c\dot{L}_{c2}\gamma_c - (\rho_{cg}-\rho_{cf})A_c\dot{L}_{c1} \tag{B2}$$

$$\Delta\dot{m}_{c3} = -\left(\frac{\partial\rho_{c3}}{\partial P_c} + \frac{1}{2}\frac{\partial\rho_{c3}}{\partial h_{c3}}\frac{dh_{cf}}{dP_c}\right)A_c L_{c3}\dot{P}_c - \frac{1}{2}\frac{\partial\rho_{c3}}{\partial h_{c3}}A_c L_{c3}\dot{h}_{co} - A_c(\rho_{cf}-\rho_{c3})(\dot{L}_{c1}+\dot{L}_{c2}) \tag{B3}$$

Substituting these equations into equation (22) and combining the similar terms together, then equation (22) can become

$$\begin{aligned}\left((\frac{\partial\rho_{c1}}{\partial P_c} + \frac{1}{2}\frac{\partial\rho_{c1}}{\partial h_{c1}}\frac{dh_{cg}}{dP_c})L_{c1} + \frac{d\rho_{cf}}{dP_c}(1-\gamma_c)L_{c2} + \frac{d\rho_{cg}}{dP_c}\gamma_c L_{c2} + (\frac{\partial\rho_{c3}}{\partial P_c} + \frac{1}{2}\frac{\partial\rho_{c3}}{\partial h_{c3}}\frac{dh_{cf}}{dP_c})L_{c3}\right)A_c\dot{P}_c + (\rho_{c1}-\rho_{c3})A_c\dot{L}_{c1} \\ + \left((\rho_{cg}-\rho_{cf})\gamma_c + (\rho_{cf}-\rho_{c3})\right)A_c\dot{L}_{c2} + \frac{1}{2}\frac{\partial\rho_{c1}}{\partial h_{c1}}A_c L_{c1}\dot{h}_{ci} + \frac{1}{2}\frac{\partial\rho_{c3}}{\partial h_{c3}}A_c L_{c3}\dot{h}_{co} + \dot{m}_{co} - \dot{m}_{ci} = 0\end{aligned} \tag{B4}$$

Furthermore, substituting three variables $\Delta\dot{m}_{c1}, \Delta\dot{m}_{c2}$ and $\Delta\dot{m}_{c3}$ described by equations (B1), (B2) and (B3) into equations (16), (18) and (20), respectively, those equations become

$$\begin{aligned}\left((\frac{\partial\rho_{c1}}{\partial P_c} + \frac{1}{2}\frac{\partial\rho_{c1}}{\partial h_{c1}}\frac{dh_{cg}}{dP_c})(h_{c1}-h_{cg}) + \frac{1}{2}\frac{dh_{cg}}{dP_c}\rho_{c1} - 1\right)A_c L_{c1}\dot{P}_c + \frac{1}{2}\left(\frac{\partial\rho_{c1}}{\partial h_{c1}}(h_{c1}-h_{cg}) + \rho_{c1}\right)A_c L_{c1}\dot{h}_{ci} \\ + \rho_{c1}(h_{c1}-h_{cg})A_c\dot{L}_{c1} + \dot{m}_{ci}(h_{cg}-h_{ci}) = Q_{csp}\end{aligned} \tag{B5}$$

$$\begin{aligned}\left((\frac{\partial\rho_{c1}}{\partial P_c} + \frac{1}{2}\frac{\partial\rho_{c1}}{\partial h_{c1}}\frac{dh_{cg}}{dP_c})h_{cg}L_{c1} + (\frac{d(\rho_{cf}h_{cf})}{dP_c}(1-\gamma_c) + \frac{d(\rho_{cg}h_{cg})}{dP_c}\gamma_c - 1)L_{c2} + (\frac{\partial\rho_{c3}}{\partial P_c} + \frac{1}{2}\frac{\partial\rho_{c3}}{\partial h_{c3}}\frac{dh_{cf}}{dP_c})h_{cf}L_{c3}\right)A_c\dot{P}_c \\ + \frac{1}{2}\frac{\partial\rho_{c3}}{\partial h_{c3}}A_c L_{c3}h_{cf}\dot{h}_{co} + \frac{1}{2}\frac{\partial\rho_{c1}}{\partial h_{c1}}A_c L_{c1}h_{cg}\dot{h}_{ci} + \dot{m}_{co}h_{cf} - \dot{m}_{ci}h_{cg} = Q_{ctp}\end{aligned} \tag{B6}$$

$$\begin{aligned}\left((\frac{\partial\rho_{c3}}{\partial P_c} + \frac{1}{2}\frac{\partial\rho_{c3}}{\partial h_{c3}}\frac{d\rho_{cf}}{dP_c})(h_{c3}-h_{cf}) + \frac{1}{2}\frac{dh_{cf}}{dP_c}\rho_{c3} - 1\right)A_c L_{c3}\dot{P}_c \\ + \frac{1}{2}\left(\frac{\partial\rho_{c3}}{\partial h_{c3}}(h_{c3}-h_{cf}) + \rho_{c3}\right)A_c L_{c3}\dot{h}_{co} + A_c\rho_{c3}(h_{cf}-h_{c3})(\dot{L}_{c1}+\dot{L}_{c2}) + \dot{m}_{co}(h_{co}-h_{cf}) = Q_{csub}\end{aligned} \tag{B7}$$

Finally, the model of the condenser can be represented by the above four governing equations (B4) - (B7), which can also be rewritten into a matrix form (23).

Acknowledgements

This work was supported by National Research Foundation of Singapore under the grant NRF2011 NRF-CRP001-090.

Reference

[1] Zhu Y, Cai W, Wen C, Li Y. Simplified ejector model for control and optimization. Energy Conversion and Management 2008; 49:1424-1432.

[2] He S, Li Y, Wang R. Progress of mathematical modeling on ejector. Renewable and Sustainable Energy Reviews 2009; 13:1760-1780.

[3] Lin C, Cai W, Li Y, Yan J, Hu Y. Pressure recovery ratio in a variable cooling loads ejector-based multi-evaporator refrigeration system. Energy 2012; 44: 649-656.

[4] Chou C, Yang P, Yan C. Maximum mass flow ratio due to secondary flow choking in an ejector refrigeration system. International Journal of Refrigeration 2001; 24:486-499.

[5] Chen W, Liu M, Chong D, Yan J. A 1D model to predict ejector performance at critical and sub-critical operational regimes. International Journal of Refrigeration 2013; 36:1750-1761.

[6] Jahangeer K, Tay AA, Raisul Islam M. Numerical investigation of transfer coefficients of an evaporatively-cooled condenser. Applied Thermal Engineering 2011; 31:1655-1663.

[7] Bendapudi S, Braun JE, Groll EA. Dynamic model of a centrifugal chiller system – model development, numerical study, and validation. ASHRAE Transactions 2005; 111:132–148.

[8] Schurt LC, Hermes CJ, Neto AT. A model-driven multivariable controller for vapour compression refrigeration systems. International Journal of Refrigeration 2009; 32:1672-1682.

[9] He X, Liu S, Asada HH. Modeling of vapor compression cycles for multivariable feedback control of HVAC systems. Journal of Dynamic Systems Measurement and Control-Transactions of the ASME 1997; 119:183–191.

[10] Rasmussen BP. Dynamic modeling and advanced control of air conditioning and refrigeration systems. PhD thesis, Department of Mechanical Science and Engineering, University of Illinois at Urbana - Champaign, 2005.

[11] Bendapudi S, Braun JE, Groll EA. A comparison of moving-boundary and finite-volume formulations for transients in centrifugal chillers. International Journal of Refrigeration 2008; 31:1437–1452.

[12] Li B, Alleyne AG. A dynamic model of a vapor compression cycle with shutdown and start-up operations. International Journal of Refrigeration 2010; 33:538-552.

[13] Catano J, Zhang T, Wen J, Jensen MK, Peles Y. Vapor compression refrigeration cycle for electronics cooling – Part I: Dynamic modeling and experimental validation. International Journal of Heat and Mass Transfer 2013; 66: 911-921.

[14] Yao Y, Huang M, Chen J. State-space model for dynamic behavior of vapor compression liquid chiller. International Journal of Refrigeration 2013; 36:2128-2147.

[15] Ding X, Cai W, Duan P, Yan J. Hybrid dynamic modeling for two phase flow condensers. Applied Thermal Engineering 2014; 62:830-837.

[16] Zhou R, Zhang T, Catano J, Wen J, Michna G J, Peles Y, Jensen M K. The steady-state modeling and optimization of a refrigeration system for high heat flux removal. Applied Thermal Engineering 2010; 30:2347-2356.

[17] Jensen JM, Tummescheit H. Moving boundary models for dynamic simulations of two-phase flows. 2nd International Modelica Conference 2002; Proceedings: 235-244.

[18] Catano J. Dynamic modeling and advanced control of vapor compression cycles for electronics cooling. PhD thesis, Department of Mechanical, Aerospace and Nuclear Engineering, Rensselaer Polytechnic Institute, 2011.

[19] Zhu Y, Cai W, Wen C, Li Y. Numerical investigation of geometry parameters for design of high performance ejectors. Applied Thermal Engineering 2009; 29:898-905.

[20] NIST Chemistry WebBook, NIST standard reference database number 69, June 2005 release. http://webbook.nist.gov/chemistry/.

[21] Vakiloroaya V, Ha Q, Skibniewski M. Modeling and experimental validation of a solar-assisted direct expansion air conditioning system. Energy and Buildings 2013; 66:524-536.